Annual Cycle of Hygroscopic Properties and Mixing State of the Suburban Aerosol in Athens, Greece.

Christina Spitieri[1], Maria Gini[1], Martin Gysel-Beer [2] and ~~Kostas~~ Konstantinos Eleftheriadis[1]

[1] Environmental Radioactivity Laboratory, Institute of Nuclear and Radiological Science & Technology, Energy & Safety, NCSR Demokritos, 15310 Ag. Paraskevi, Athens, Greece
[2] Laboratory of Atmospheric Chemistry, Paul Scherrer Institute, Forschungsstrasse 111, Villigen PSI, Switzerland

Correspondence to: Christina Spitieri (spitieri@ipta.demokritos.gr) and Maria Gini (gini@ipta.demokritos.gr)

Abstract. The hygroscopic properties of atmospheric aerosol were investigated at a suburban environment in Athens, Greece, from August 2016 to July 2017. The Growth Factor Distribution Probability Density Function, (GF-PDF), and mixing state were determined with a Hygroscopicity Tandem Differential Mobility Analyzzer, (HTDMA). Four dry particle sizes, (D_0), were selected to be analyzzed in terms of their hygroscopic properties at 90 % relative humidity. The annual mean GFs for D_0 =30, 50, 80, and 250 nm, were found to be equal to 1.28, 1.11, 1.134, and 1.22, respectively. The hygroscopic growth spectra werecan be divided into two distinct hygroscopic ranges; a non and/or slightly hygroscopic mode (GF<1.12) and a moderately hygroscopic mode (GF>1.12), which are representative of a suburban environment influenced by local/urbanregional emissions and background aerosol. The standard deviation σ of the GF-PDF was employed as a measure of the mixing state of ambient aerosol. The 30 nm particles were mostly internally mixed, whereas larger particles were found to be externally mixed, with either a distinct bimodal structure or with partly overlapping modes. Cluster analysis on the hourly dry number size distributions measured in parallel, was performed to identify provided the link between aerosol hygroscopicity and aerosol emission sources and formation processesgrowth/evaporation dynamics. The size distributions were classified into five groups, with the "mixed, urban and aerosol background" aerosol (67%) and "urban-nocturnal" aerosol (12%) to account for 79% of the results. The hygroscopic properties for 50 nm and 80 nm were found to be similar in all cases, indicating particles of similar nature and origin across these sizes. This was also confirmed through the modal analysis of the average number size distributions for each cluster; the 50 nm and 80 nm particles were found to belong to the same Aitken mode in most cases. The 250 nm particles (i.e. accumulation mode) were generally more hygroscopic than Aitken particles, but less hygroscopic than the 30 nm particles (nuclei mode).

Introduction

Atmospheric aerosol particles in the ambient atmosphere affect the radiation budget of the planet and the regional and global climate (IPCC, 2013; Rosenfeld et al., 2014), through direct and indirect effects (Li et al., 2016). As a direct effect, Aaerosol

particles interact with solar radiation through light absorption and scattering, inducing a positive or negative radiation forcing, respectively (Haywood and Boucher, 2000)~~., (direct effect of aerosol).~~ ~~As an indirect effect,~~ Additionally, aerosol particles can act either as cloud condensation nuclei (CCN) or as ice nuclei (IN), which determines their indirect effect on ~~affecting~~ cloud's microstructure and lifetime. The climate-relevant properties of atmospheric aerosol particles are largely influenced by their ability to take up water, (hygroscopicity), and their state of mixing~~, by their size and chemical composition.determined by their size, chemical composition, hygroscopicity and state of mixing~~ (Zhang et al., 2011; Kaufman et al., 2002; McFiggans et al., 2006).

The hygroscopic properties of atmospheric particles are strongly related to particle chemical composition (Gunthe et al., 2009; Gysel et al., 2007), while they undergo continuous changes over particle lifetime. Research results have shown that the relative non-hygroscopic fresh organic aerosol can ~~be converted to~~ become hygroscopic through physical and chemical atmospheric processes (Kanakidou et al., 2005). This is also the case for soot particles originating from different sources (e.g. biomass burning, diesel soot). Condensation of secondary species~~–~~ on the surface of primarily emitted soot, (pure black carbon particles)~~on the particle phase and on going coagulation~~, may alter their hygroscopic properties ~~of soot particles~~ from non-hygroscopic, to hygroscopic ~~with the latter~~ being therefore capable to act as CCN (Tritscher et al., 2011; Kotchenruther and Hobbs, 1998). Motos et al., (2019) also studied and established the relations ~~quantified the link~~ between the black carbon core size, ~~and~~ mixing state and droplet activation.

Aerosol hygroscopic growth can be measured or estimated by both direct and indirect techniques (Dean A. Hegg et al., 2007, P. Achtert et al., 2009). The most widespread real-time direct measurement technique for fine mode aerosol is the Hygroscopicity Tandem Differential Mobility Analyzer, (HTDMA), which determines the G~~g~~rowth F~~f~~actor, (GF), of particles at a given dry particle diameter and relative humidity, (RH). Then, the hygroscopic parameter κ, a simplified parameter model the composition-dependence ~~–~~of the solution water activity can be calculated as described by Peter and Kreidenweis (2007~~),). in order to investigate the hygroscopic properties of aerosol due to their chemical composition which allows to infer basic information on the chemical composition of the aerosol, though typically not fully unambiguous (Bezantakos et al., 2013; Gysel et al., 2007).~~ The kappa values for highly hygroscopic aerosols, such as salts and sulfates, range between 0.5 and 1.4, for organics from 0.01 to 0.5, whereas for non – hygroscopic aerosol such as soot, the kappa values are close to zero (Bezantakos et al., 2013; Gysel et al., 2007).

The cloud nucleating effectivity of aerosol particles and the overall aerosol-cloud-climate interactions, depend on the distribution of components among individual particles, termed as "aerosol mixing state" (Riemer et al., 2019). Ambient aerosol is usually considered a heterogeneous mixture of particles with different chemical compositions and sizes. We refer to an internal mixture of aerosol when the particles of the same size have similar chemical composition. Whereas, in an external mixture particles of the same size have distinctly different chemical composition. The aerosol in urban/sub-urban environment~~ss~~ typically is an external mixture of non-hygroscopic aerosol from fresh local emissions and moderately hygroscopic background aerosol (Wang et al., 2018; Enroth et al., 2018; Swietlicki et al., 2008~~–~~), whereas in marine environments the aerosols tend to be internally mixed and highly hygroscopic (Massling et al., 2007).

Long-term measurements of aerosol hygroscopicity are commonly done using CCN counters (e.g. Paramanov et al., 2015, Schmale et al. 2017, Schmale et al., 2018 and references therein) or HTDMAs. A few long term studies of aerosol hygroscopicity and mixing state by means of the HTDMA technique have been published so far, and some of them are mentioned below ~~useful for the better understanding of the link between particle hygroscopic growth and particle emission sources, formation and transformation processes. A few long term studies of aerosol hygroscopicity and mixing state by means of the HTDMA technique have been published so far, and some of them are mentioned below~~ (Kammermann et al., 2010, Fors et al., 2011, Holmgren et al. 2014). These provide a better understanding of the link between particle hygroscopic growth and particle emission sources, formation and transformation processes. ~~Long-term measurements of aerosol hygroscopicity are useful to better identify the aerosol properties with respect to particle emission sources, formation and transformation processes, with few detailed HTDMA studies available so far (Kammermann et al., 2010, Fors et al., 2011, Holmgren et al. 2014).~~ The present study aims at providing insights into the hygroscopic properties and state of mixing of ambient aerosol and the origin of ambient ultrafine and fine particles, through 1 year of measurements of key microphysical parameters (i.e. size distributions and time- and size- resolved HTDMA data) in a suburban environment. The hygroscopicity of ambient aerosol was investigated in the particle size range between 30 and 250 nm, providing information about the month-to-month variability, seasonal cycle and diurnal pattern of hygroscopicity and the degree of mixing state for selected particle sizes. ~~of the suburban aerosol in Athens.~~

2. Methodology

2.1 Sampling Site

The measurement campaign was conducted from August 2016 to July 2017, at the Demokritos (DEM) station (fig.1.), member of GAW and part of the ACTRIS and PANACEA infrastructures within the National Centre of Scientific Research Demokritos campus. The station is located in~~,~~ ~~a~~ a vegetated area at the foot of Mount Hymettus, about 7~~8~~ km to the North east from Athens city centre. It is an urban background station, representative of the atmospheric aerosol in the suburbs of the Athens Metropolitan Area. The site is partially influenced by transported pollution from the urban area of Athens (Eleftheriadis et al., 2021) (i.e. under most atmospheric conditions) and partially by the incoming regional aerosol (i.e. under Northern, Southern or Eastern winds).

Figure 1 The Demokritos Atmospheric Aerosol Measurement station in Athens, (from © Google Maps).

2.2 Instrumentation

A custom-built Humidified Tandem Differential Mobility Analyzer, (HTDMA), was used to measure the hygroscopic growth factor distributions of ambient aerosol particles with selected dry diameters, D_0, at certain narrow size fractions centered around 30 nm, 50 nm, 80 nm and 250 nm and exposed at relative humidity (RH) of 90 ± 2 %, (Bezantakos et al., 2013). Figure 2 shows the main components of the HTDMA system. The HTDMA consists of two differential mobility analyzers (DMAs) in tandem mode, a humidifier section and a condensation particle counter, (CPC 3772, TSI). The polydisperse aerosol was initially dried, passing through an aerosol Nafion dryer, and brought to charge equilibrium passing through a ^{85}Kr bipolar neutralizer, before entering the first DMA, (DMA-1), where the specific particle sizes were selected, (monodisperse aerosol), according to their electrical mobility. Then, the monodispersed and dried particles were conditioned, by passing through the humidifier section, at a well-defined relative humidity (set point 90 %), before entering the second DMA (DMA-2); the sheath flow of the DMA-2 was also humidified at a relative humidity of 90 %. The DMA-2 was operated with the CPC in a scanning mobility sizer configuration, (SMPS), to measure the particle size distribution of the conditioned wet aerosol. Both DMAs were operated with a sheath flow rate of 3 L/min, and a sample flow rate of ~0.3 L/min. ~~The DMA$_2$ was operated in line with the CPC in a scanning particle mobility sizer configuration, (SMPS), to measure the particle size distribution of the conditioned wet aerosol.~~

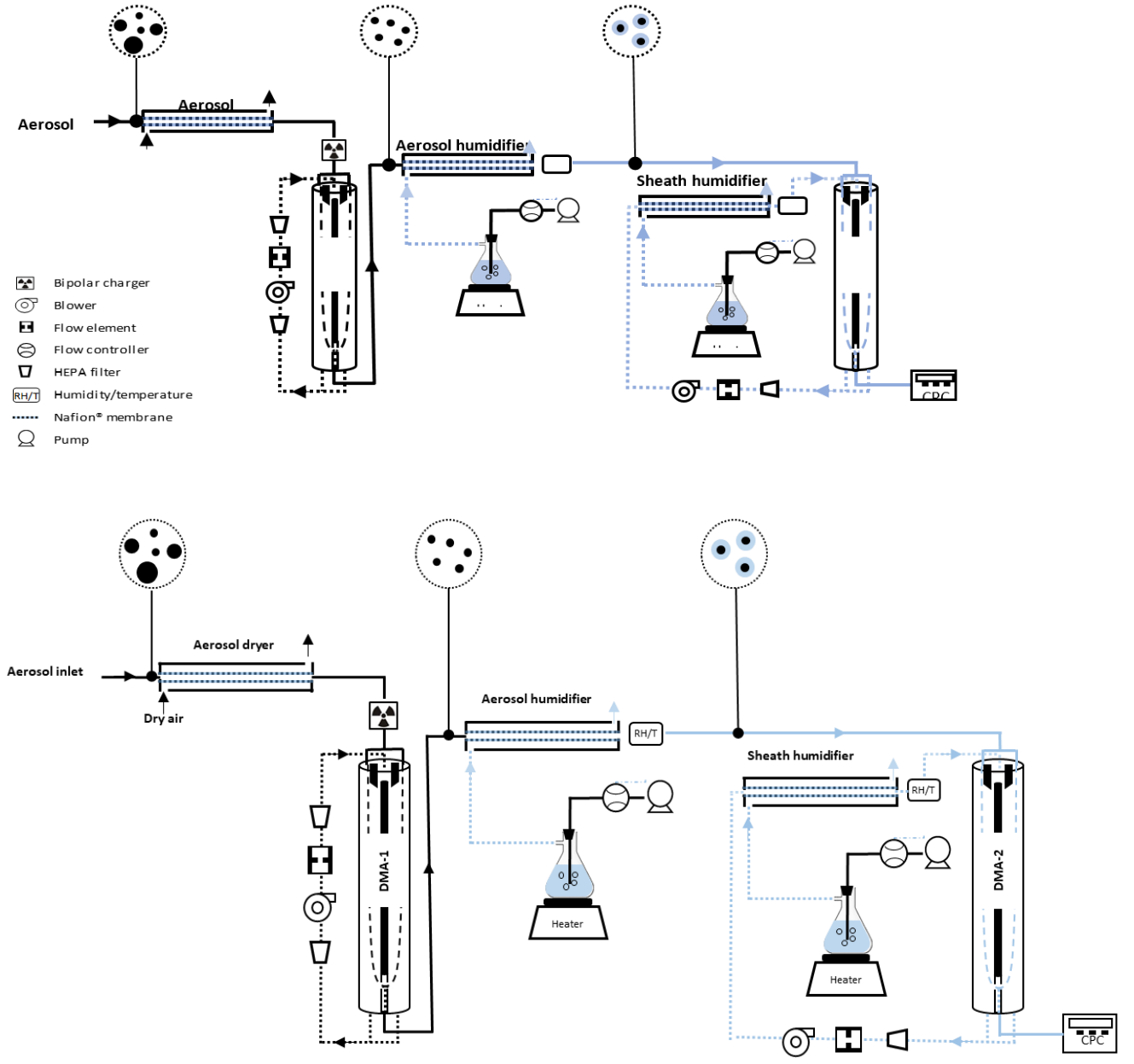

Figure 2 Schematic diagram of the HTDMA system

115

The aerosol number size distributions of ambient aerosol, (dry), were measured by means of a Scanning Mobility Particle Sizer system (SMPS), operated in parallel with the HTDMA at the DEM station. ~~The aerosol number size distributions of ambient aerosol (dry) were measured in parallel by the standard SMPS system of the DEM station,~~ The SMPS consists of ~~with five~~

~~minute time resolution, consisting of~~ an electrostatic classifier (TSI Inc. model 3080), a cylindrical differential mobility analyzer column, (TSI Inc, model 3081), and a condensation particle counter, (TSI Inc., model 3772). It~~The SMPS~~ was operated with a five-minute time resolution and ~~at~~ an aerosol-to-sheath flow ratioe of 1/5 lpm ~~and a sheath flow rate 5 lpm,~~ covering~~extending the measured~~ a particle size range from 10 nm to 550 nm. Both, aerosol and sheath, ~~SMPS~~ flows were dried to relative humidity lower than ~~35~~ 40% using a Nafion drier. Data acquisition and analysis was performed using the ~~non-commercial~~ TROPOS-SMPS data evaluation software, (Wiedensohler et al., 2012). To achieve the highest measurement accuracy with SMPS measurements, the technical recommendations and quality control procedures proposed by Wiedensohler et al. (2012) were followed.

The standard meteorological parameters (i.e. temperature, humidity, wind speed and, ~~wind direction and solar radiation~~) were recorded at an hourly time interval at DEM station. The meteorological sensors were installed on a meteorological mast, at 10 m height above ground.

2.3 Data analysis

2.3.1 HTDMA data inversion and fitting procedure

Due to water uptake, the diameter of the humidified particles (D(RH)) increase, and the ratio between humidified, (D(RH)), and dry particle diameter, D_0, is defined as the Growth Factor (GF):

$$GF = \frac{D(RH)}{D_0}, \quad (1)$$

w~~W~~here, D(RH) is the particle diameter at the given RH and D_0 is the dry diameter selected by the first DMA. The particle concentration at the HTDMA outlet as a function of G~~g~~rowth F~~f~~actor, (GF), set at the HTDMA is referred to as Measurement Distribution Function, (MDF).

Then, an inversion algorithm was applied to the measured MDF to retrieve the actual G~~g~~rowth F~~f~~actor P~~p~~robability D~~d~~ensity F~~f~~unction~~s~~ (GF-PDF), which describe the probability that a particle with a defined dry size exhibits a certain GF at the specified relative humidity. The methodology we follow for inverting the HTDMA data is described in detail by Gysel et al. (2009). A key element for the data inversion is the Kernel function, which describes the physics of a ~~the HTDMA~~TDMA system ~~instrument~~. The Kernel width calibration, for particles exhibiting a true growth factor of 1.0, of the HTDMA and data inversion, ~~using TDMAinv algorithm,~~ were performed according to the methodology described by Gysel et al. (2009), applying the TDMAinv algorithm~~.~~. The underlying principle of the HTDMA inversion approach~~es~~ is to find an inverted GF-PDF, such that a minimum χ^2 ~~x^2~~-residual is obtained between the measured MDF and the reconstituted MDF, (R-MDF). The G~~g~~rowth F~~f~~actor

Pprobability Ddensity Ffunctions (GF-PDFs) were afterwards normalized to unity. The GF-PDFs measured in the range 887 % < RH < 92 % were recalculated to RH = 90 % following the procedure described by Gysel et al. (2009), in order to minimize reduce uncertainties associated with RH variations in RH levels. Each GF-PDF was described as a piecewise linear function with the midpoint of the first and last inversion bin at GF=0.7 and GF=2.5, respectively, and a resolution of ΔGF=0.1. The GF standard deviation, σ, of a GF-PDF, was also determined according to Eq. (C.6) in Gysel et al. (2009).

The σ is used as a measure for the spread of growth factor to describe the mixing state (Sjogren et al., 2008).

In the present study, the inverted datadata -were can be grouped into three cases, representative of the aerosol mixing state in fig. 3. Indicative inverted GF-PDFs are presented in Fig. 3., reflecting the three cases of mixing state. Specifically, σ ≤0.07 indicates an internally mixed aerosol (fig.3, Panel (A), σ ≥ 0.15 describes an externally mixed aerosol with two distinct modes (fig.3, Panel (C), whereas GF-PDFs with 0.07 < σ <0.15 -are considered as a continuum of mixing states with two overlapping modes or a broad mode (fig.3, Panel (B), (almost bimodal and externally mixed). The bimodal GF-PDFs spectra, either with overlapping or with well-defined modes, was divided into two distinct ranges of particle hygroscopicity: one subset comprising non and/or slightly hygroscopic particles with GF<1.12, the other subset comprising moderately hygroscopic particles with GF>1.12. This threshold GF coincides with the typical local minimum in the GF-PDFs observed in this study, which also is in line with the findings of previous studies (Kim et al., 2020). Then the different integral properties of GF-PDFs (i.e. mean GF and number fraction), for these subranges, were calculated by Eq. (C.9) and Eq. (C.8), as described by Gysel et al., 2009, by averaging GF-PDFs above and below the GF = 1.12 threshold. It has be noted that a sensitivity analysis has been performed before selecting the two subranges, by changing the selected threshold GF between1.12 and 1.20 with no significant effect on the calculated parameters. The fixed GF threshold translates to slight size dependence of the kappa threshold, i.e. from 0.1107 to 0.1205 for 30 to 250nm. Overall, the GF-PDFs appeared to have either two distinct GF modes, one in the GF < 1.12 subset and one in the GF > 1.12 subset (often the case for particles in the accumulation size range), or partially to fully overlapping GF modes, (often the case particles in the Aitken mode).

The mean GF and the number fraction of particles of each mode was calculated by Eq. (C.9) and Eq. (C.8), respectively, in Gysel et al., 2009.

Additionally, the hygroscopicity parameter κ, was calculated as follows (Petters and Kreidenweis, 2007):

$$\kappa = \frac{(GF^3 - 1)(1 - a_w)}{a_w} \quad \kappa = \frac{(GF_3 - 1)(1 - a_w)}{a_w} \qquad (2)$$

where a_w is the water activity, at which the growth factor was measured. According to Köhler theory (Köhler, 1936), a_w is obtained by

$$a_w = \frac{RH}{exp(\frac{4\sigma_S v_w}{RTD})} \qquad (3)$$

where σ_s is the surface tension of the solution droplet (assumed to be pure water), v_w is the partial molar volume of water in solution, R is the universal gas constant, T is the temperature, and D is the diameter of the droplet.

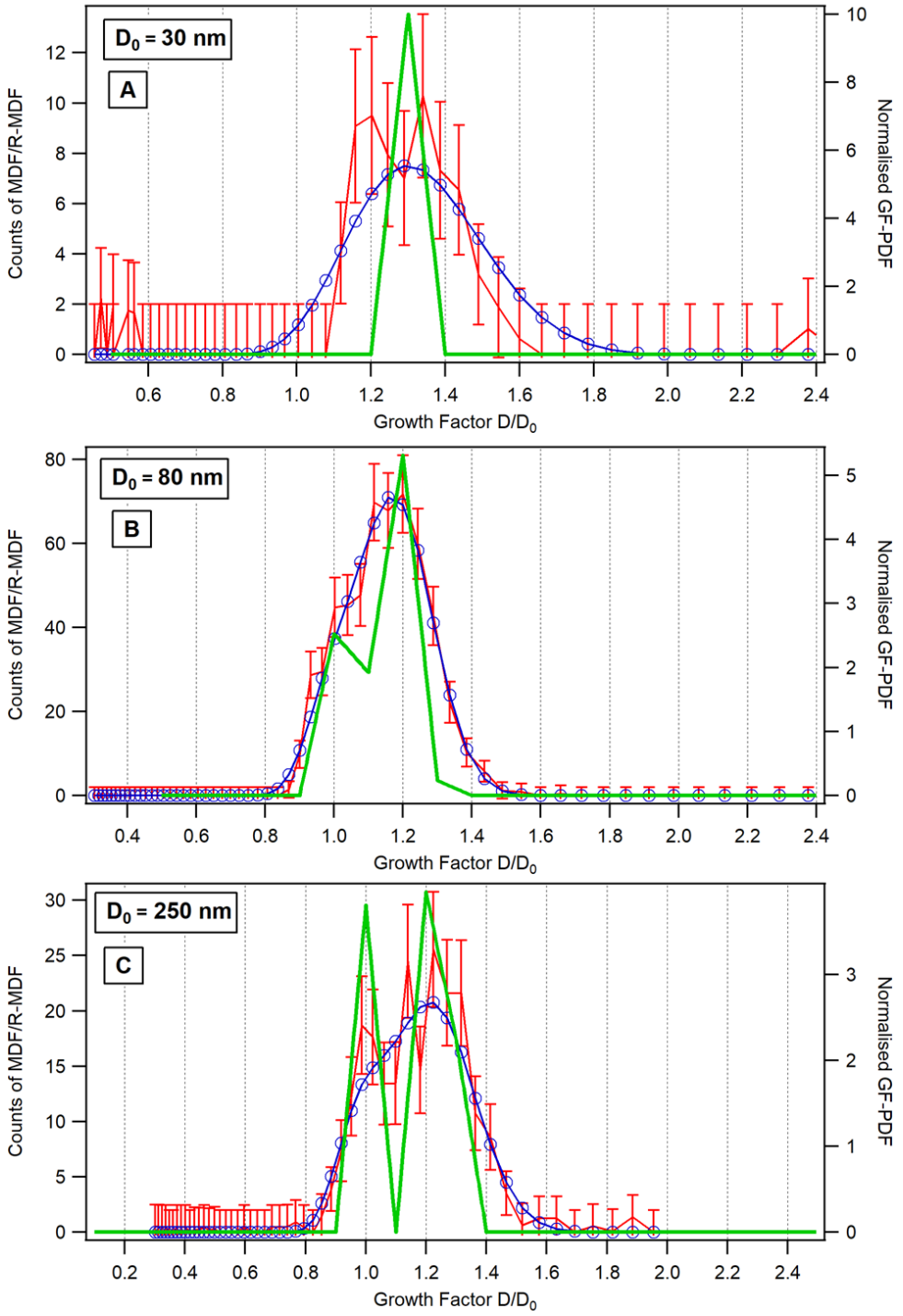

Figure 3 Example of growth factor distributions measured at RH=90% of D_0=30nm particles (Panel (A), internally mixed), of D_0=80nm particles (Panel (B), continuum of mixing states) and of D_0=250nm particles (Panel (C), externally mixed with distinct modes). The red line

represents the measured particle counts, the blue line represents the reconstructed measured distribution function and the green line is the GF-PDF.

2.3.2 Cluster Analysis

k-means cluster analysis was applied to the hourly-average particle number size distributions to classify the distributions of the highest degree of similarity into the same cluster, reducing in that way the complexity of the dataset. The k-means method aims to minimize the sum of the squared Euclidian distance between each dataset point and the corresponding cluster center (i.e. the mean of all the points in a cluster). Cluster analysis was performed using the IBM SPSS software. The interpretation of the origin of each cluster was based on the dominant size modes (Hussein et al., 2014), their hourly frequency of occurrence and the average values obtained for standard meteorological parameters.

2.3.3 Multimodal Analysis

The modal characteristics of the clustered average number size distributions were obtained by applying a curve-fitting algorithm as proposed by Hussein et al. (2005). The least squares method was used to best-fit the sum of up to 4 modes to the multi-modal distributions to the clustered number size distributions. The log-normal distributions were described by the following characteristic modal parameters of each mode: ~~i.e.~~ geometrical mean mobility diameter, number concentration and geometric standard deviation. Starting from an initial assumption, the modal parameters of each log-normal distribution were successively re-defined to obtain the best-fit curve. The algorithm starts by fitting a uni-modal log-normal distribution, and successively tests the possibility of increasing it to a bi-, a tri- and finally a tetra-modal distribution. The optimum best-fit curve was determined by minimizing the root mean square error (RMSE, %), defined as ~~described by~~ Vratolis et al. (2019).

$$RMSE = \frac{100}{\sqrt{n}} \left(\sum_{i=1}^{n} (N_{dpi}^{m} - N_{dpi}^{f})^2\right)^{0.5} \quad (4)$$

where, n is the number of size bins of the SMPS size distribution, N_{dpi}^{m} is the number concentration measured by the SMPS at size bin i corresponding to particle diameter dpi, and N_{dpi}^{f} is the number concentration of the sum of fitted modes at diameter dpi.

3. Results and Discussion

3.1 Seasonal and monthly variability of aerosol GF and mixing state

The seasonal, as well as the annual, mean GF-PDFs, fig. 4., were calculated by averaging the individual GF-PDF for each dry particle size~~, split by~~ and season. The GF-PDFs represent the mean distributions of the growth factors of particles with D_0=30, 50, 80 and 250nm.~~,~~ The selected dry sizes are ~~which are~~ representative of the nuclei ~~mode~~ (30nm), Aitken ~~mode~~ (50 and 80nm) and accumulation ~~mode~~ (250nm) mode of the aerosol number size distributions, respectively. It has to be highlighted that the mean~~.~~ GF-PDFs represent the mean distributions of growth factors and does not necessarily provide a clear picture of the mixing state of these size fractions. In specific, the appearance of a broad mode or two overlapping~~ed~~ modes or two distinct modes does not imply the simultaneously existence of particles with distinctly different hygroscopic properties and therefore compositions, but it may also result as a matter of GF temporal variability. Below it will be further discussed and clarified which factor is the prominent one at different cases. ~~However, some broadening of the modes in the GF-PDF and the shape of GF-PDF results from the calculation of averages. This does not necessarily provide a clear picture of the mixing state of these size fractions, when modal GF varies over time.~~ The majority of the mean GF-PDFs of the nuclei mode particles with dry diameters of 30 nm were characterized by a unimodal peak, during all seasons,~~(~~ except from winter~~)~~, with GFs to be ranged between 1.17~~20~~ and 1.41, as reported in Table S1. Non and/or slightly hygroscopic 30-nm-particles with GF~1.0 are essentially missing, in contrast to particles with D_0>30nm,~~.~~ indicating that ~~freshly emitted particles, such as~~ bare black carbon particles do not make a dominant contribution at this size either because sources of other particle types are stronger or because they rapidly acquire some hygroscopic coatings. ~~, are probably growing faster to sizes larger than 30 nm, and are observed as such largely absent during most of the year with the exception of winter, (January & February). AAging processes are not very effective during the dark and colder months, therefore a small fraction of non hygroscopic carbonaceous fresh aerosol is very likely to remain and be detected in these below 30 nm size fraction. It has been found that these aging processes are more efficient for the nuclei mode rather than the higher Aitken modes in modifying their hygroscopicity due to condensation of organics and inorganics onto the pre-existing particles (Vu et al., 2011).~~ In winter, the existence of two modes indicates that probably both fresh, (non and/or slightly hygroscopic), and aged, (moderately hygroscopic), emissions from traffic and other combustion sources, (biomass burning, residential heating), contribute to the 30 nm size fraction. In general, the aging processes are more efficient for the nuclei mode rather than the higher Aitken modes in modifying their hygroscopicity ~~in modifying their hygroscopicity~~ due to condensation of organics and inorganics onto the pre-existing particles (Vu et al., 2021). The fact that 30nm aerosol particles are characterized as externally mixed only during wintertime is a combined effect of the time scale of the aging process, which is not very effective during the dark and colder months, and the relative contributions ~~time scale of mixing~~ of fresh and background aerosol at the background location of the DEM station. More detailed discussion for this fraction will follow further below.

~~Also BC is simply bigger than 30nm, and therefore whatever is in the nucleation mode is already little bit hygroscopic, and at the bigger sizes one could have the more hygroscopic material condensed on BC cores or even the pure BC particles as well.~~

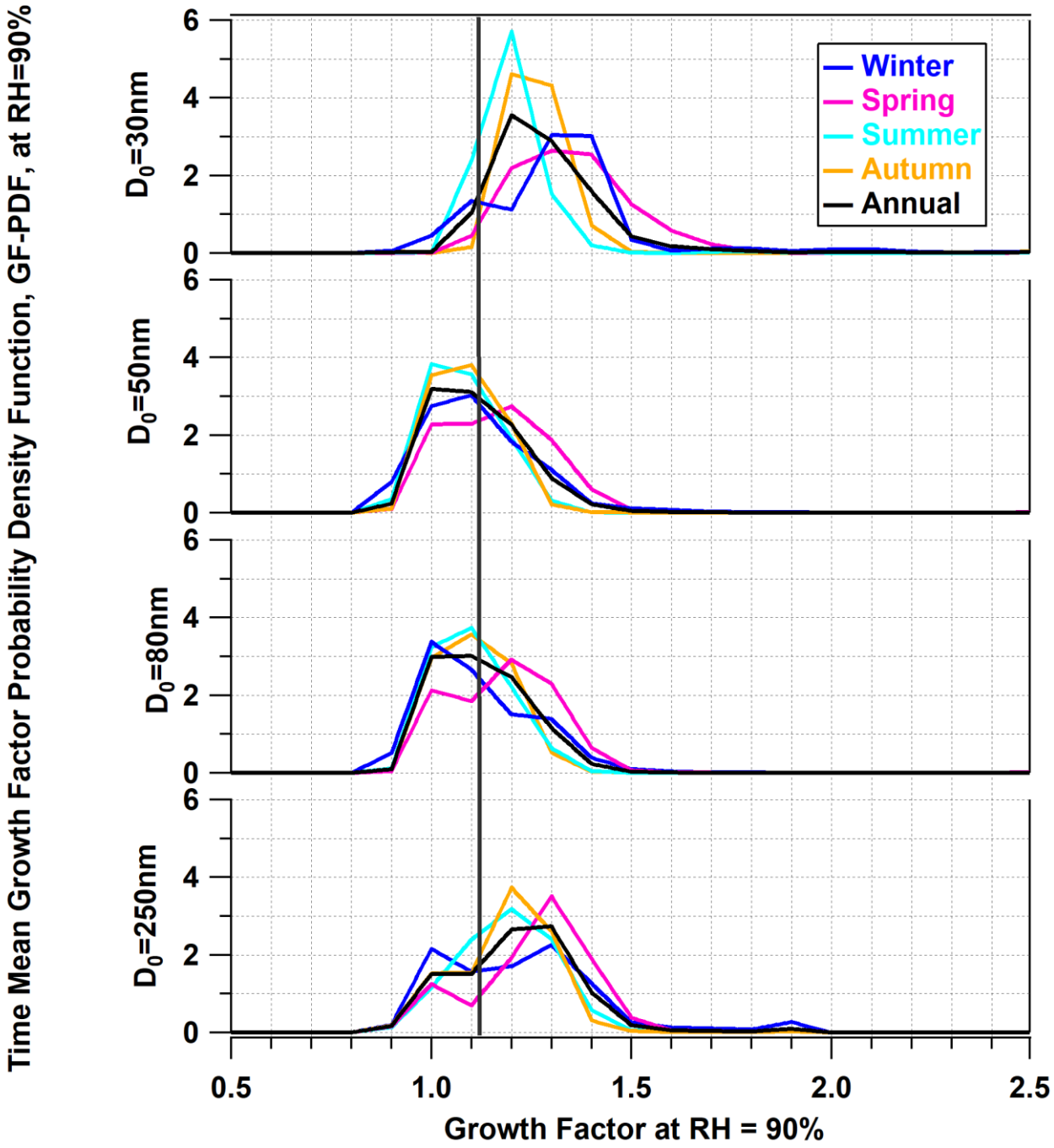

255

Figure 4 Seasonal and annual mean GF-PDFs for different dry particle sizes (30, 50, 80 and 250 nm). The vertical black line represents the selected cut-off between the- non and/or slightly hygroscopic mode (GF<1.12) and the moderately hygroscopic mode (GF>1.12).

The existence of a broad mode in the GF-PDF of 30nm particles in winter provides the expected aerosol phenomenology that both fresh (non or slightly hygroscopic), aged (moderately hygroscopic) emissions from traffic and other combustion sources (biomass burning, residential heating) and hygroscopic fraction from the occasional nucleation events of local or distant origin contribute to the 30 nm fraction. The fact that all the above are visible only in the two winter months is the combined effect of the time scale of the aging process and the time scale of mixing of fresh and background aerosol at the background location of the DEM station. One must consider that during winter weaker aging results from the lowest temperatures and lowest photochemical activity experienced in Athens. More detailed discussion for this fraction will follow further below.

The GF-PDFs of medium to large Aitken mode particles, i.e. at 50 nm and 80 nm, characterized by a broad peak, within the range of display a low degree of external mixing, with average GF ranges between 1.00 and 1.273, (Table S1). The contribution of the non and/or slightly hygroscopic mode and moderately hygroscopic particles make almost equal contributions to the GF-PDF, indicating that the contribution of non or slightly hygroscopic particles is higher in the Aitken mode compared to the moderately hygroscopic mode in all seasons, except spring. than the 30nm particles.

The separation of the two distinct hygroscopic modes, (a bimodal distribution or a continuum of mixing states), is most pronounced for the accumulation mode particles, (250 nm). The contribution of the moderately hygroscopic mode to the total hygroscopicity is higher compared to the hygroscopicity of Aitken particles. Particles larger than 100 nm are usually more aged than the smaller particles, with higher values of GF (Cubison et al., 2006), and more immediately associated with the atmospheric processing they undergo during long-range transport (Kalivitis et al., 2015). However, in winter time the expected slowing down of secondary aerosol formation processes and the existence of larger primary particles, partly from biomass burning (Bernardoni et al., 2017), make evident the distinct appearance of the fresh non and/or slightly hygroscopic mode and moderately hygroscopic mode in this size range.s. Moreover, looking at the GF-PDFs of the particles in the accumulation mode a peak appeared in the highly hygroscopic range. However, the number fraction corresponding to at peak is so low that is unimportant to identify the true nature of this negligible small peak. close to zero and does not appear to be physically meaningful. It can only be considered as an artefact of the inversion code.

Laborde et al., (2013) also showed that the particles with GF<1.12 themselves can be an external mixture of BC rich and organic rich particles, in this peculiar case associated with local/regional traffic and wood burning emissions probed at a peri-urban site of Paris. The background aerosol was found to be more hygroscopic in their case compared to this study. In August, GF-PDFs were unimodal across the size range 50 nm $\leq D_0 \leq$ 250 nm, and the mean GF was as low as 1.03 to 1.09. Such dominance of non or slightly hygroscopic particles suggest that the Aitken and accumulation mode aerosol was dominated by non or slightly -hygroscopic BC potentially affected by nearby forest fires (Carrico et al., 2005).

The annual mean growth factors at 90 % relative humidity were found to be 1.28, 1.11, 1.14 and 1.22 for D_0 = 30, 50, 80 and 250 nm, respectively. Although a distinct month-to-monthseasonal variability was observed on the average GFs. Monthly mean values of hygroscopicity parameter κ, determined according to Equations (1) and (2), were found to be 0.13, 0.05, 0.05 and 0.09 for particles with dry diameters 30, 50, 80 and 250 nm, respectively, with a distinct month to month variability,

In order to investigate the hygroscopic properties of particles in more detailed~~4~~, the temporal variability of mean GF, ~~(Panels A-D), of GF~~ of standard deviation, σ, ~~(Panels E-H),~~ of individual GF-PDF measurements and of ~~hygroscopicity~~hygroscopicity parameter κ, ~~(Panels I-L),~~ was assessed by means of the box plots presented in fig. 5. for each month and~~,~~ for the ~~the~~ dry ~~diameters~~ diameteres-, 30, 50, 80 and 250nm.

~~A first peak in GF was observed during spring time (April – May) and the second peak during late autumn-early winter., there was no distinct seasonal variability on the average GFs. It has to be empathized that apparent features with higher values in spring may partly be over-emphasized by the August feature, which likely is driven by a meteorological outlier rather than being a representative feature of the aerosol typically encountered in August.~~ ~~In a further analysis, the uncertainty and error analysis of the variation of GF percentiles of the GF-PDF, are presented as box plots in fig. 6, for each month, for the dry diameters 30, 50, 80 and 250nm. Monthly mean values of hygroscopicity parameter κ, determined according to Equations (1) and (2), were found to be 0.13, 0.05, 0.05 and 0.09 for particles with dry diameters 30, 50, 80 and 250 nm, respectively, with a distinct month to month variability, (fig. 5. Panel B). Panel C in fig. 5. shows the monthly variation of the standard deviation, σ, for all particle sizes, describing the mixing state of aerosol (Rose et al., 2010).~~ The 30nm particles appeared to have a peak in GF during spring time, (April - May), and a second peak during late autumn-early winter, with a high variability in mean GF, (fig.5, Panel A). The 30nm particles ~~The 30 nm particles are~~ were internally mixed for all months with $\sigma \leq 0.07$, except from January and February, where the mean σ was 0.10 and 0.13, respectively~~,~~ (fig.5, Panel B). In the latter case the aerosol particles ~~are~~ were externally mixed, (overlapping modes). Despite the fact that the monthly mean GF-PDFs in fig.S1 look similarly broad in February and April, the time-resolved data are quite different. In April the 30nm particles are characterized by low degree of mixing state, (always low sigma, $\sigma = 0.07$~~8~~), while considerable temporal variability in mean GF leads to a broad monthly mean GF-PDF. By contrast, in February, the mean GF exhibits limited variability, while the aerosol is externally mixed at any time ($\sigma = 0.13$). The κ values corresponding to the mean GFs ~~,~~ranged from 0.11 to 0.33, (fig.5, Panel C).

~~The mPanel C, ranged between 0.11 and 0.33and presented similar variation patterns as the mean GFs, with the higher values occurring during the transition seasons, (spring and fall), and the lowest occurring in winter and summer.~~ The Aitken particles (50 and 80 nm) were characterized by a continuum of mixing states (externally mixed with overlapping modes), with σ values (fig.5, Panels E and H) ranging between 0.09 and 0.13, except from August, where the mean σ was 0.06, indicating an internally mixed aerosol. On average, the mean GFs and κ values of the Aitken particles appeared to follow the same trend as~~have the same seasonal variation of mean GF (Panels D and G, respectively), with~~ the 30nm particles but with lower absolute values.~~,~~ The κ ~~although were (Panels x and x),~~ values of the Aitken particles, (fig.5, Panels F and I, respectively), ~~as can been seen from the values of the parameter κ (Panels x and x), which~~ ranged between 0.02~~x~~ and 0.13. ~~temporal variability,.Although, κ values for the particles with D_0=50 and 80nm are lower than this of 30nm particles, in agreement with lower mean GFs.~~

~~-~~The D_0=250 nm particles ~~do not appeared to have a distinct seasonal variability of mean GF (Panel x), except from August and September, where GF values are minimum. Although, 250nm particles~~ were characterized by a high degree of external mixing state, ($0.09 \leq \sigma \leq 0.16$, Panel K~~x~~), during all months, except of August and September where the aerosol display a low degree of mixing state (σ=0.09). The mean GF and ~~The hygroscopicity parameter~~ κ values were minimum in August, (1.09,

0.03, respectively), and maximum in April, (1.29, 0.13, respectively), ~~(Panel x), ranged between x and x,~~ indicating the seasonal variability in ~~different~~ chemical composition of ambient aerosol throughout the year. ~~particles in the accumulation mode (externally mixed with distinct modes).~~

A higher degree of external mixing state in winter (February), was generally expected due to less effective aging process. Exact magnitude and timing at this seasonal effect remains elusive based on a single year of observations.

~~In short, the highest spread of GFs was observed in February, for all dry diameters, indicating a mixture of a fresh and aged emissions and background aerosol. In contast, lowest σ values were observed in August, indicating the existence of internally mixed aerosol in nuclei and Aitken modes, whereas the particles in the accumulation mode remain externally mixed although with a lower degree of mixing.~~

~~Mean κ values, determined according to Equations (1) and (2), were similar for particles with D_0 >30nm, as shown in fig.5 Panels I L, indicating the existence of the same chemical compounds.~~ ~~The particles in the Aitken mode (50 and 80 nm) appeared to be characterized by a continuum of mixing states (externally mixed) with σ values ranging between 0.09 and 0.13, except from August, where the mean σ was 0.06 indicating an internally mixed aerosol. The D_0=250 nm particles were characterized by a high degree of external mixing (0.09 ≤ σ ≤ 0.16), during all months, except of August where the aerosol display a low degree of mixing state (σ=0.09).~~ The annual mean growth factors at 90 % relative humidity were found to be 1.28, 1.11, 1.13 and 1.22 for D_0 = 30, 50, 80 and 250 nm, respectively. The mean values of hygroscopicity parameter κ, determined according to Equations (1) and (2), were found to be 0.22, 0.06, 0.08 and 0.12 for particles with dry diameters 30, 50, 80 and 250 nm, respectively.

~~In August, the GF PDFs were almost unimodal across the whole size range between 50 nm and 250 nm, and the mean GF was as low as 1.03 to 1.09. Such dominance of non or slightly hygroscopic particles suggest that the Aitken and accumulation mode aerosol might be dominated by mostly primary particles related to fresh carbonaceous emissions.~~

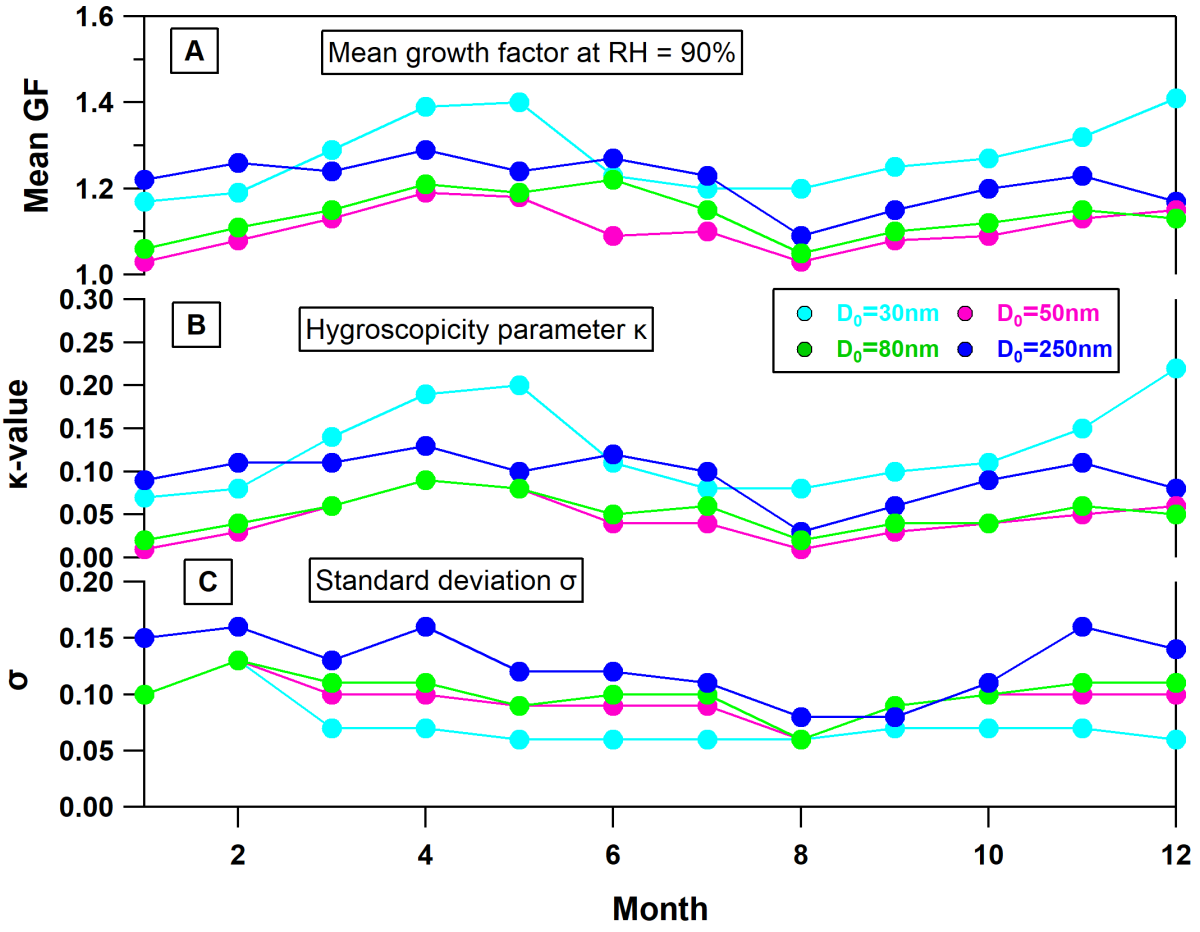

Figure 5 Annual cycles A) of the mean growth factor (GF) at 90% RH, B) of the corresponding hygroscopicity parameter κ, C) of the monthly mean standard deviation σ, for different particle sizes

In Figure 6, the monthly boxplots of σ values are presented. For particle dry sizes D_0 > 30 nm, a distinct variability in the degree of mixing state was observed, from month to month. The highest spread of GFs was observed in February, implying the co-existence of traffic- and biomass burning- related emission sources. In contast, smaller σ values were observed in August, indicating the existence of internally mixed aerosol in nuclei and Aitken modes, whereas the particles in the accumulation mode remain externally mixed although with a lower degree of mixing.

In general, the Aitken particles and the particles in the accumulation mode (D_0 > 30 nm) and the particles in the accumulation mode can be characterized as an external mixture of moderately hygroscopic (aged) and non hygroscopic aerosol (i.e. background aerosol mixed with regional and local emissions, respectively).

~~The bimodal GF-PDFs spectra, either with overlapping or with well-defined modes, was divided into two distinct ranges of particle hygroscopicity: one subset comprising non-hygroscopic and slightly hygroscopic particles with GF<1.12, the other subset comprising moderately hygroscopic particles with GF>1.12. Mean properties of each subset were calculated by averaging GF-PDFs above/below this threshold GF of 1.12. This threshold GF coincides with the typical local minimum in the GF-PDFs observed in this study, which also is in line with the findings of previous studies (Kim et al., 2020). Note, sensitivity analyses performed by changing the selected threshold GF of 1.12 to 1.20 had a very little effect on the calculated parameters. The particles with GF below/above the threshold can be present as distinct GF modes, often the case for the accumulation mode size range, or partially to fully overlapping GF modes, often the case for the smaller sizes within the Aitken mode.~~

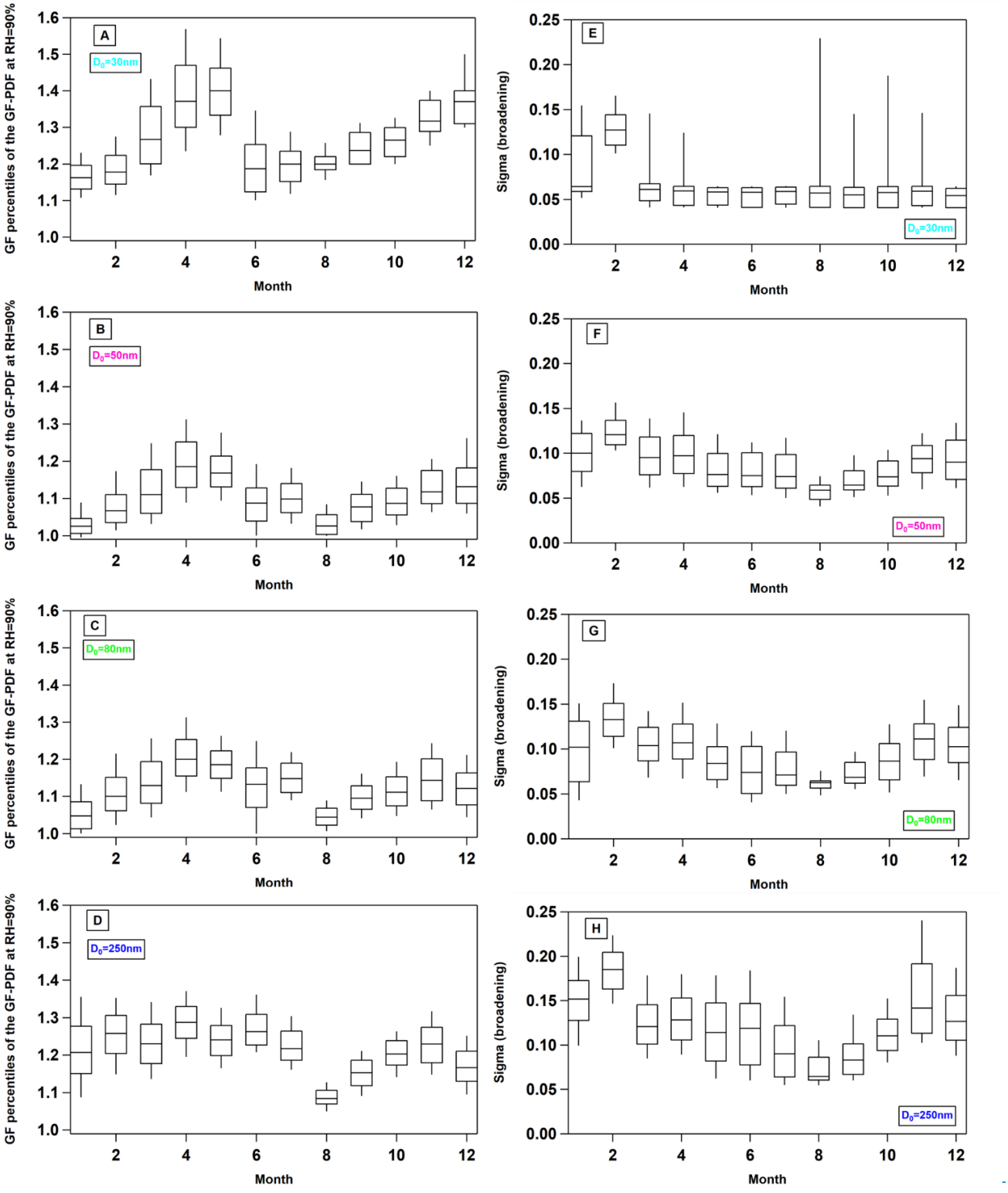
A
D_0=30nm
B
D_0=50nm
C
D_0=80nm
D
D_0=250nm
E
D_0=30nm
F
D_0=50nm
G
D_0=80nm
H
D_0=250nm
GF percentiles of the GF-PDF at RH=90%
Sigma (broadening)
Month

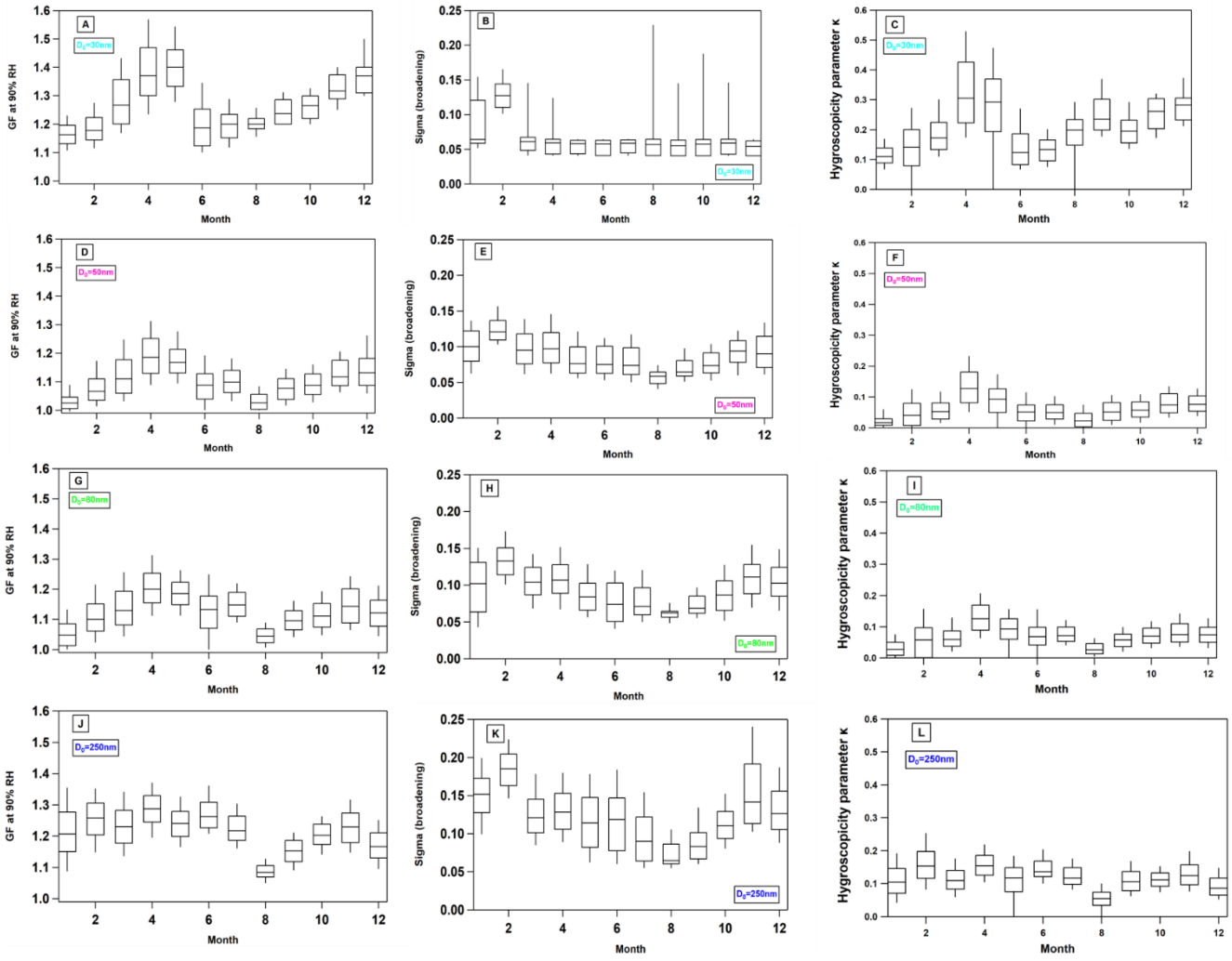

370

Figure 5~~6~~ Percentiles of the GF-PDF, ~~and~~ standard deviation, σ, and hygroscopicity parameter κ, for each dry si~~z~~ze and for each month. Box plots with whiskers show 10th, 25th, 50th, 75th and 90th percentiles.

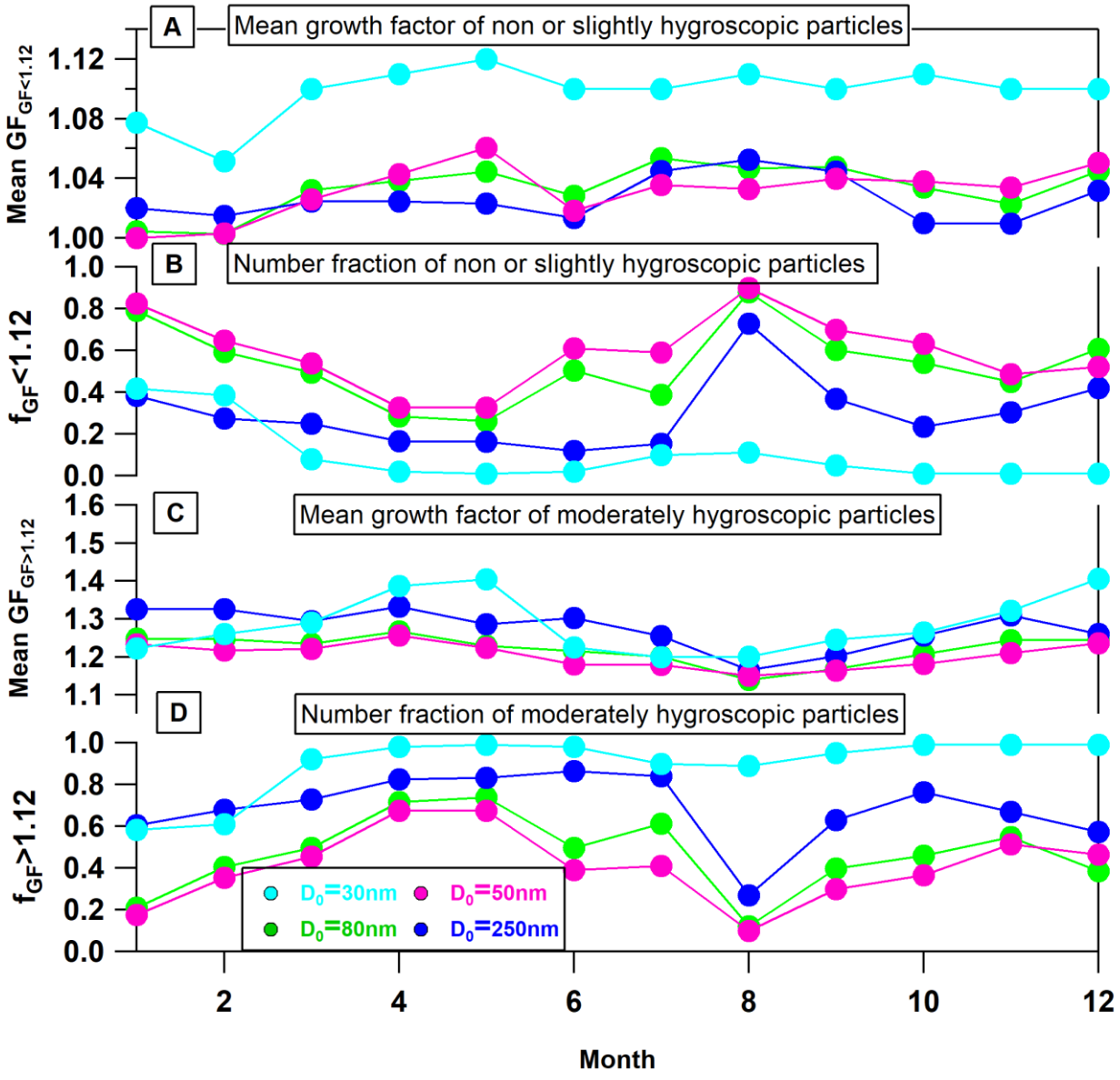
A
Mean growth factor of non or slightly hygroscopic particles
Mean GF GF<1.12
1.12
1.08
1.04
1.00
B
Number fraction of non or slightly hygroscopic particles
f GF<1.12
1.0
0.8
0.6
0.4
0.2
0.0
C
Mean growth factor of moderately hygroscopic particles
Mean GF GF>1.12
1.6
1.5
1.4
1.3
1.2
1.1
D
Number fraction of moderately hygroscopic particles
f GF>1.12
1.0
0.8
0.6
0.4
0.2
0.0
D0=30nm
D0=50nm
D0=80nm
D0=250nm
2
4
6
8
10
12
Month

375

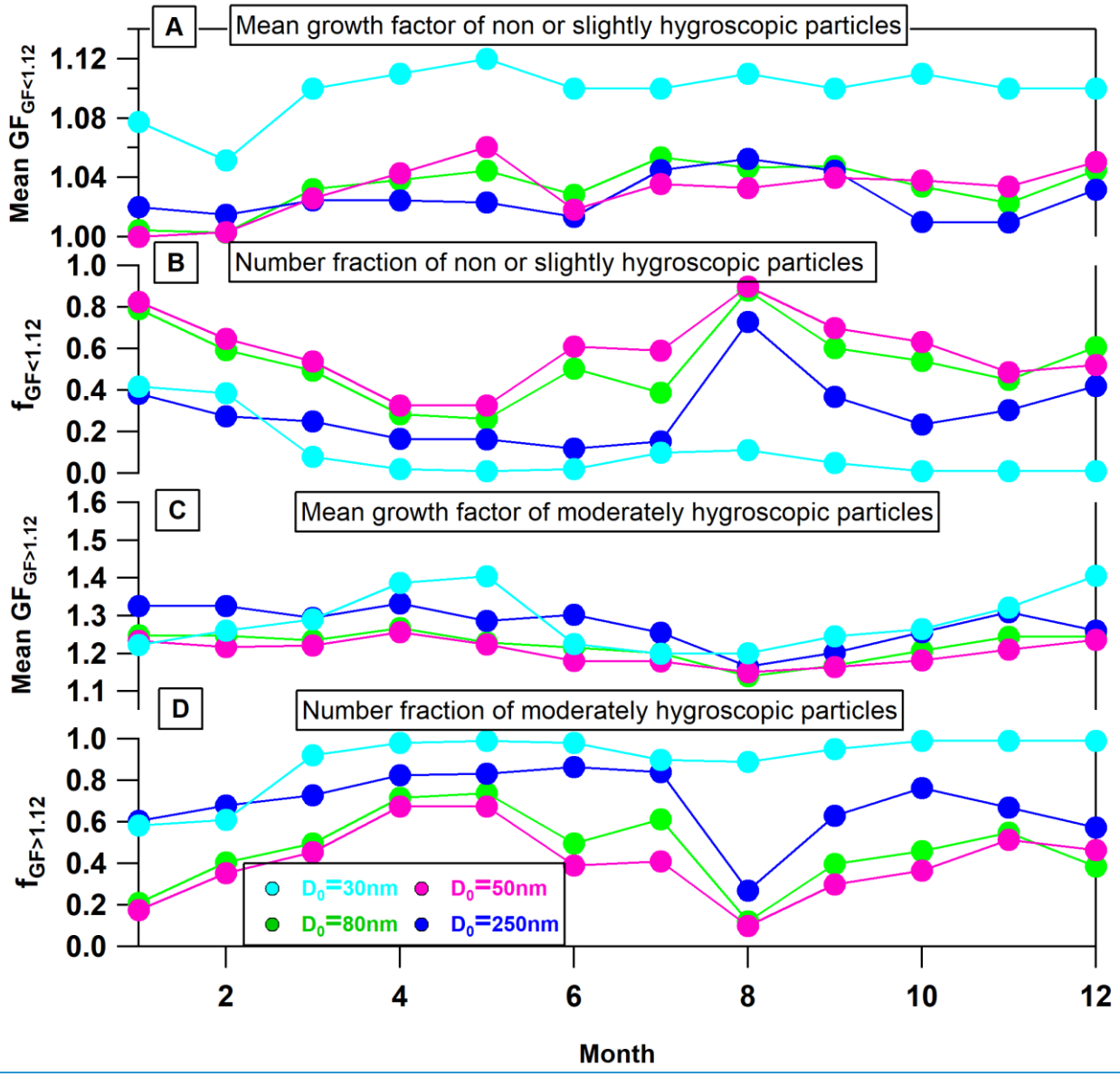

Figure 6~~7~~ Annual cycles A) of the monthly mean GFs for non- or slightly hygroscopic particles at 90% RH, B) of number fraction of non- and/or slightly hygroscopic particles at 90% RH, C) of the monthly mean GFs for moderately hygroscopic particles at 90% RH, and D) of number fraction of moderately hygroscopic particles, for different particle sizes.

Figure 6~~7~~ shows the monthly mean GFs and the number fraction, f_{GF}, of non and/or slightly hygroscopic and moderately hygroscopic mode, for each D_0. The variation of the mean GF for particles with GF < 1.12 is expected to be relative low, given that the upper boundary of the non and/or slightly hygroscopic mode, (1.12), is quite low and close to the lowest boundary, (1.0). ~~Whereas, T~~the mean GF of the moderately hygroscopic mode presented larger variability, with the minimum to be

observed in summer, (i.e. August). for particles with D_0>30 nm. In short, The mean GF of the subset with GF>1.12 was larger for the 30 nm and 250 nm particles compared with the 50 and 80 nm particles. The different hygroscopic properties of these particles reflect the ir differences in their t chemical compositions, with the particles in the nucleation and in the accumulation modes with the nuclei particles and the particles in the accumulation mode containing a larger fraction of more hygroscopic compounds, such as inorganics and more oxidized organics, compared to Aitken particles (Bougatioti et al., 2016)., than that of Aitken particles. This trend in the size dependence of the mean average GFs and consequently of the mean kappa values, for the Aitken and accumulation modes is in line with the results from previous studies (Xu et al., 2019; Juranyi et al., 2013; Petäjä et al., 2007). Indicative GFs values for different chemical compounds are listed in Table 12. for different chemical compound classes. Table S1 summarizes the monthly mean GFs at RH=90 %, the mean GF of each mode, along with the hygroscopicity parameter κ and the number fraction of each mode, for dry diameters 30, 50, 80 and 250 nm.

The number fraction of each mode also significantly varied from month to month for all dry sizes, with distinct variability in the relative contributions of particles with small or moderate-to-large growth factors. For Specifically, for dry particle diameters D_0 > 30 nm, the contribution of the non- and and//or slightly hygroscopic mode was maximum minimum in spring and maximum in August and and minimum in winter. In the case of Aitken particles, the non-hygroscopic particles almost equal contributed to aerosol hygroscopicity with the slightly hygroscopic particles in all seasons except for spring. This implies higher contribution of fresh and regional aerosol in the Aitken mode compared to the accumulation mode. For particles with D_0 = 250 nm, the moderately hygroscopic particles clearly dominate over those with GF<1.12 for all seasons. Specifically, the average number fraction of the slightly moderately hygroscopic particles with D_0 = 250 nm, were 0.62, 0.80, 0.67 and 0.70 in winter, spring, summer and autumn, respectively. This is consistent with the perception that the accumulation mode is dominated by aged aerosol (i.e. background aerosol), which is typically considered more hygroscopic than fresh emitted particles (Psichoudaki et al., 2018).

TABLE 12 Mean Growth Factors measured at RH=90% for cold and warm period

Chemical Composition	Growth Factor, (GF)	Source
BC, Mineral Dust	**<1.05**	**Vlasenko et al., 2005**
Biomass Burning	**1.15-1.65**	**Cocker et al., 2001**
Aged wood smoke	**1.3-1.5**	**Kotchenruther and Hobbs, 1998**
Fresh wood smoke	**1.1-1.3**	**Kotchenruther and Hobbs, 1998**
Inorganic Ions	**~1.7**	**Gysel et al., 2002**
Organic Compounds	**1.0-1.7**	**Koehler et al., 2006**

3.2 Annual and seasonal diurnal variability

The mean diurnal variability of critical meteorological parameters i.e. wind speed, temperature and relative humidity are shown in fig. S2. The daily average temperature varied between 17.2 ºC and 20.5 ºC, peaking at midday, whereas the average daily relative humidity was ~ 60%, ranging between 68%, (night and early morning), and 49%, (midday). The daily average wind speed varied between 1.81 ms^{-1} and 2.84 ms^{-1} peaking also at midday. ~~The atmosphere was relatively wet with an average daily relative humidity ~ 60% and a peak at night and early morning (~ 68%) and a minimum at midday (~ 49%).~~ Generally, higher concentrations of traffic-related pollutants are expected to be observed at the suburban site at midday, when conditions favour mixing and dispersion of the generated aerosol across the Athens valley. The prevailling~~-~~ westerly winds become~~are~~ stronger resulting in a well-mixed atmosphere, while the pollutants are transported from the city to the suburban site (Kalogridis et al., 2018). During the evening hours, a peak in the concentration levels of different air pollutant is typically observed reflecting the increased atmospheric stability ~~s peak due to the developing~~(development of ~~-~~local inversion/nocturnal boundary layer), and ~~to additional~~ emissions from different combustion sources especially in ~~by residential heating in~~ winter (i.e. residential heating), (Eleftheriadis et al., 2021).

~~In general,~~ Pparticle hygroscopicity was lower during morning rush hours, when an increase ~~peak~~ in the traffic-related emissions is expected to occur., ~~while~~ In the ~~during the~~ afternoon an increase in hygroscopicity was observed which may be attributed to the condensation of water soluble organics and inorganics on fresh primary particles of local and regional~~/regional~~ origin ~~and on background aerosol~~ (Psichoudaki et al., 2018). According to previous studies, the mass fraction of secondary organic compounds, which is generally higher in summer~~, peaks at noon~~ (Diapouli et al., 2017), peaks at noon, resulting in intermediate GF values (GF < 1.3) a few hours later (Bourcier et al., 2012).

The diurnal m~~M~~ean GFs, standard deviations of mean GF~~s~~, σ, ~~GFs~~ and number fractions of the non and/or slightly~~-~~ hygroscopic and the ~~slightly~~ moderately hygroscopic modes are presented in fig. 7~~8~~., for each dry particle ~~all particle's~~ size~~s~~. ~~-~~The Aitken particles are generally externally mixed throughout the day, with higher contribution of the moderately hygroscopic mode in the early morning (03:00-05:00). A second but less pronounced peak also appeared in the afternoon. The 24h cycle of the mean GF of the non and/or slightly hygroscopic mode (GF < 1.12), appeared to have two peaks, with the major contribution of the non and/or slightly~~-~~ hygroscopic particles to occur at midday. Particles in the accumulation mode appeared to have a somewhat similar hygroscopic behaviour, in terms of diurnal variability, with Aitken particles, even though with less pronounced changes within the day for both growth factors and number fractions. The standard deviations, σ, of subsets with GF<1.12 and GF>1.12 are presented in fig. S3.

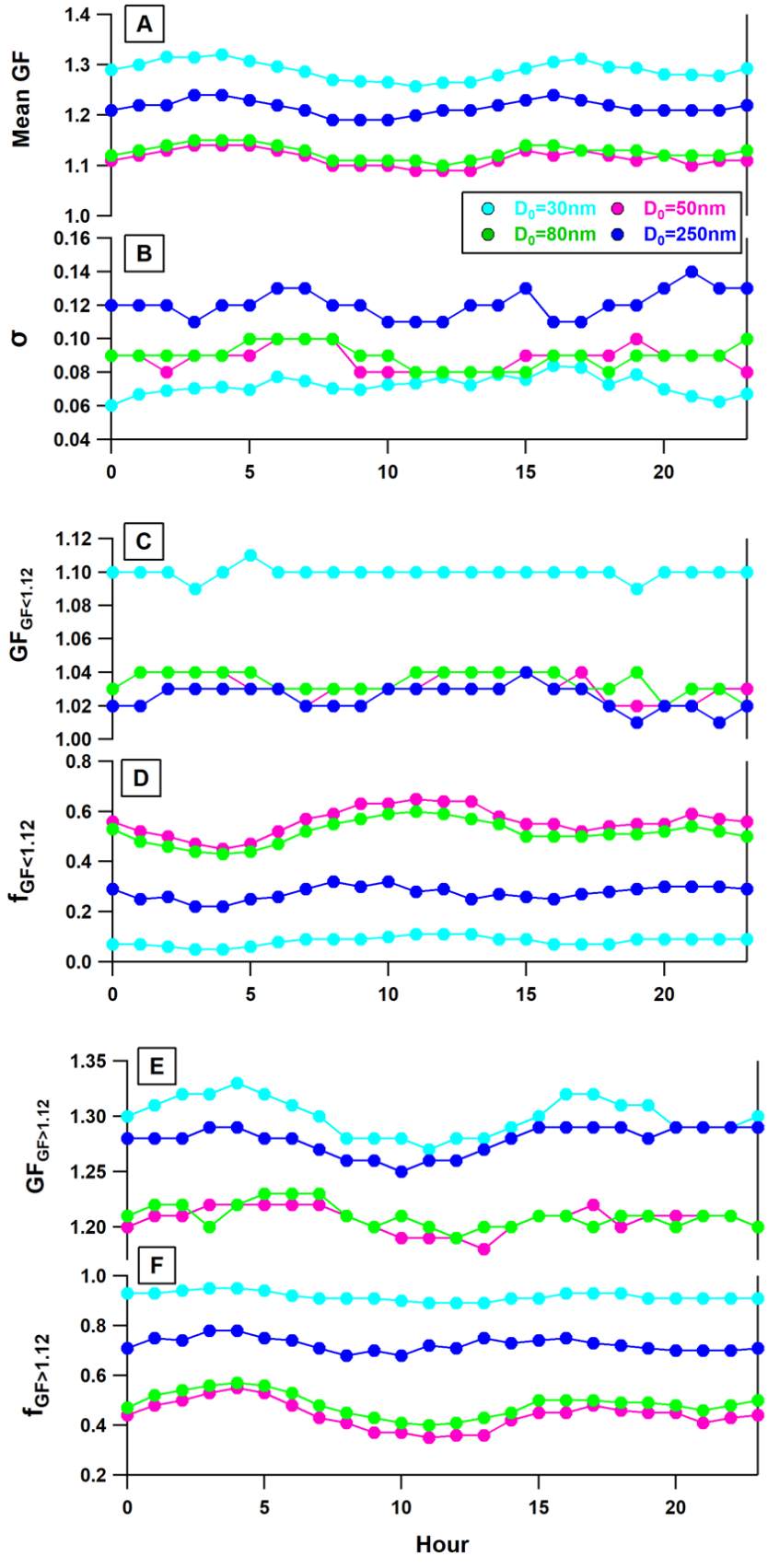
A
Mean GF
1.4
1.3
1.2
1.1
1.0
D0=30nm
D0=50nm
D0=80nm
D0=250nm
B
σ
0.16
0.14
0.12
0.10
0.08
0.06
0.04
0
5
10
15
20
C
GFGF<1.12
1.12
1.10
1.08
1.06
1.04
1.02
1.00
D
fGF<1.12
0.8
0.6
0.4
0.2
0.0
E
GFGF>1.12
1.35
1.30
1.25
1.20
F
fGF>1.12
1.0
0.8
0.6
0.4
0.2
Hour

Figure 7~~8~~ Diurnal variation of A) mean GF, measured at RH=90% , B) standard deviation of the mean GF, C) GF of non or slightly hygroscopic particles, D) the number fraction of non or slightly hygroscopic particles, E) GF of moderately hygroscopic particles, and F) the number fraction of moderately hygroscopic particles

For the 30 nm particles, it was observed that the GF of the moderately ~~slightly~~ hygroscopic mode was higher (GF > 1.3), between ~~late evening~~late evening and early morning (00:00 – 05:00 UTC+2), when the relative humidity appeared to have the maximum values (fig. S2)~~,~~ as well as at early afternoon (15:00 – 20:00 UTC+2), whereas the minimum appeared at ~~noon (GF < 1.3) (~~21:0~~0~~0 UTC+2~~)~~. At the DEM station, the 30 nm particles are generally related to traffic emissions or new particle formation (Vratolis, et al., 2019)~~., as shown~~ In ~~in~~ fig.S4, the CPF (conditional probability function) polar plot of 75th percentile of the total number concentration in the size range from ~~. for the~~ 20 to ~~-~~38nm~~-~~ is presented (Carslaw and Ropkins, 2012). It is obvious that these particles are predominately originated from the urban area, under moderate wind speeds. ~~particle population.~~ T~~t~~aking into account ~~the map of the area that 75% of the values for this size range arrive from the center of the city. Also take into account~~ that the distance between Athens city center and DEM station is around 7 km, the transport time within the Athens value at the indicative wind speeds observed are yielding estimated transport time between ½ hour to a few hours. These data provide enough evidence to assume that urban emission are the main source of these nuclei particles, while ~~and~~ adequate time for further aging is also ensured. As the particles undergo atmospheric aging their composition changes, in relative terms, due to condensation of secondary aerosol which is most pronounced for the small particles. During the photochemical active period of the day, (at noon), secondary formation of condensable organics, which might occur faster than that of inorganics, is probably responsible for the appearance of less hygroscopic Aitken particles than that of 30 nm, which is consistent with the findings presented in previous studies, (Mochida et al., 2008).

~~A special case to be considered is the hygroscopic properties of the nuclei particles in winter when these nuclei particles appeared to be externally mixed. In fig. 89, the mean diurnal variability of the number size distributions, averaged over time periods when 30 nm are were externally, (19/01/2017-28/02/2017), orand internally mixed, are presented along with the mean growth factors of the moderately modes and the number fraction of the moderately hygroscopic mode, (i.e. in the case of externally mixed), and the mean GF (i.e. in the case of internally mixed) of the 30 nm particles. As stated before, the externally mixed nature of the nuclei particles in winter, is the combined effect of the time scale of the aging and mixing processes of fresh emitted and background aerosol at the DEM station. Specifically, Tthe average number size distribution of ambient aerosol revealed enhancedstrong primary particle emissions, (i.e. increased number concentration of nuclei particles), during the traffic rush hours, from the early morning until midday. In winter these emissions ere enhanced further by biomass burning especially in the afternoon and evening. When internally mixed in the morning and in the evening when biomass burning also significantly contribute in aerosol concentrations. It can be seen than the traffic related nuclei particles emissions in the morning are related to lower contribution of moderately hygroscopic particles appeared to have the lowest hygroscopicity during the traffic rush hours in the morning midday and early evening. When externally mixed, (January and February), the~~

~~contribution of moderately hygroscopic mode was minimum during the morning traffic rush hours, but it remained relatively stable ($f_{GF>1.12}$ > 0.55) for the rest of the day, although the mean $GF_{GF>1.12}$ appeared to have the same diurnal pattern as the mean GF of the internally mixed nuclei particles. As stated before, the hygroscopic properties of the nuclei particles and their externally mixed nature in winter, reflects the combined effect of the time scale of the aging, (less efficient during winter), and mixing processes of fresh emitted and background aerosol at the DEM station.~~ than the biomass burning related ones. In the summer (absence of biomass burning emissions), traffic remains the major emission source of nuclei particles; these particles are characterized as internally mixed and of lower hygroscopicity than the aged ones.

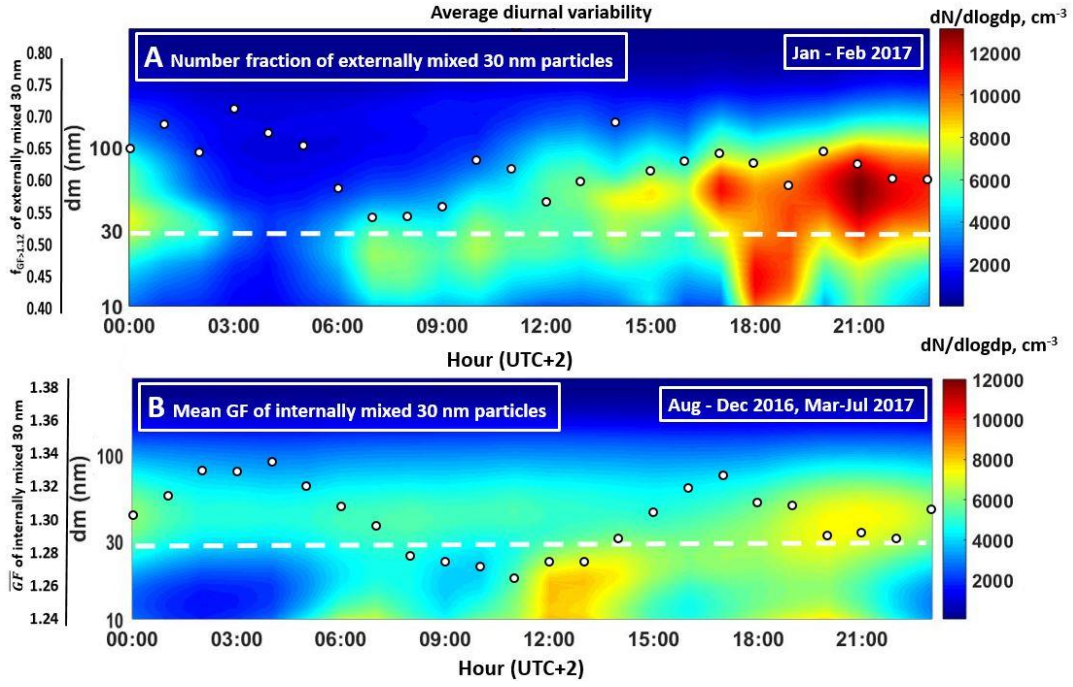

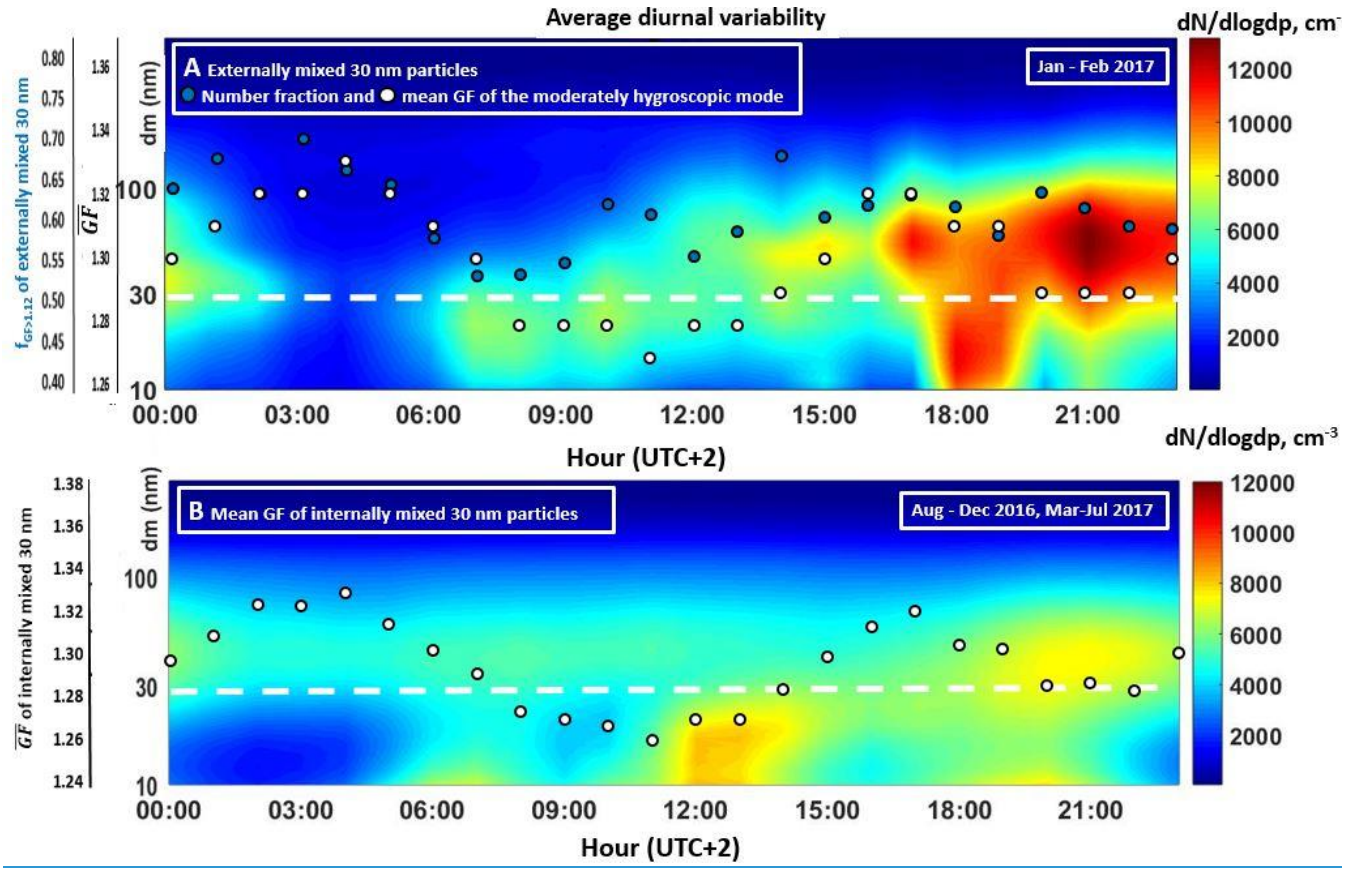

Figure 89 Diurnal variability of the average number size distributions for periods when (A) 30 nm are externally mixed (19/01/2017 - 28/02/2017). The white circles represent the number fraction of the externally mixed 30 nm particles with GF > 1.12 and (B) 30nm are internally mixed (August – December 2016, March – July 2017). The white circles represent the mean GFs and the blue circles the number fraction of the moderately hygroscopic mode in the case of the externally 30nm.of the internally mixed 30 nm particles.

Figure 910, shows the seasonally resolved diurnal patterns of the GFs of the moderately hygroscopic mode for the specific particle sizes. The 30 nm particles, appeared to have a similar diurnal pattern in all seasons, peaking in late afternoon and early morning. Though, significantly different GFs levels were observed, with the largest GFs found in winter and spring and the lowest in summer. The shape of the diurnal pattern of the larger particles with D_0 = (30, 80 and 250 nm) also depends on season. In the summer and autumn, the GFs were lower within the day, gradually increasing during nighttime (i.e. unimodal daily variability), while in winter/spring a more complex structure was observed.

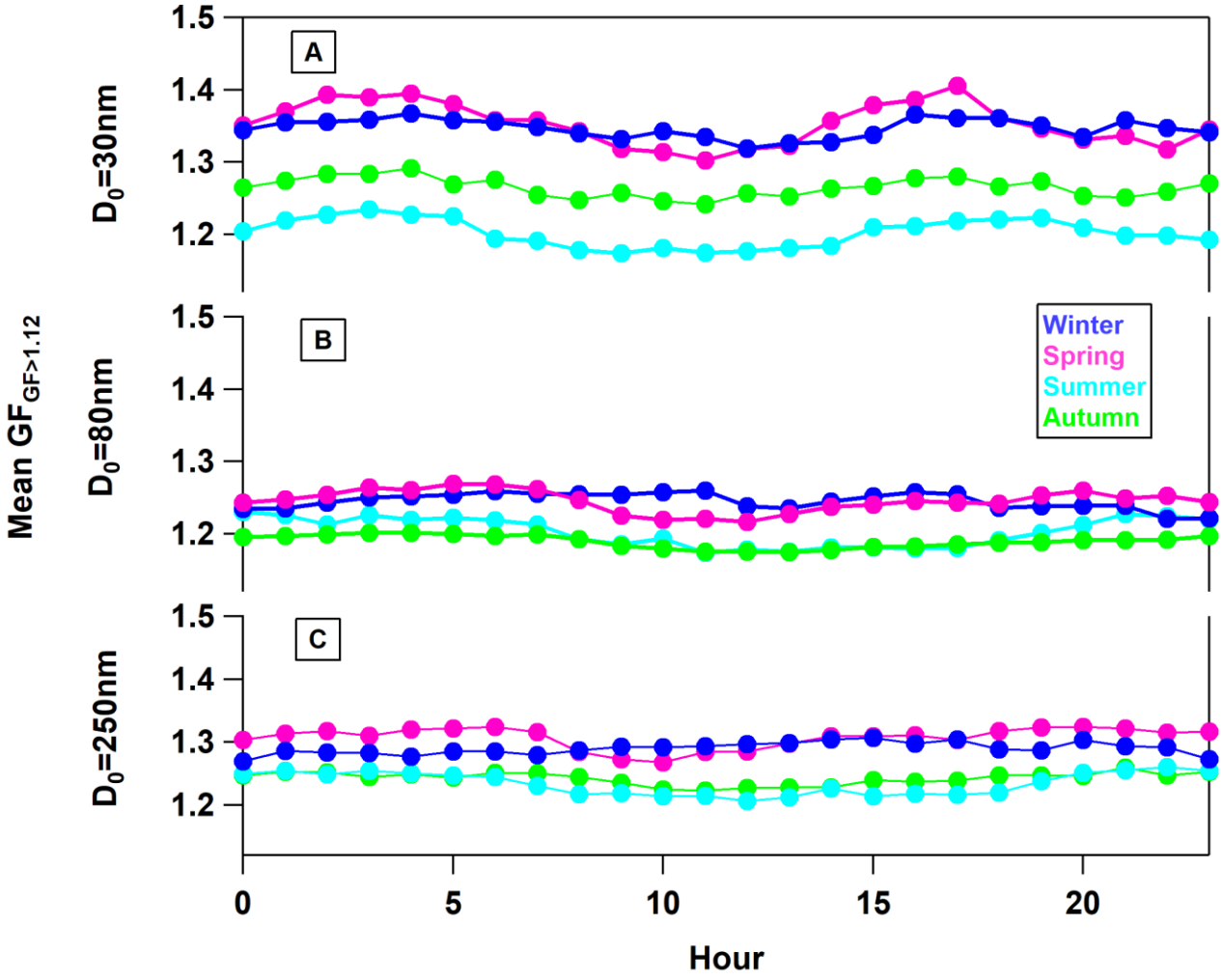

Figure 10 Diurnal variation segregated by season of the mean GF of all particles with GF>1.12 for dry diameters A) 30, B) 80 and C) 250 nm.

3.3 Cluster analysis and aerosol hygroscopic properties

Cluster analysis was performed on the hourly average size distributions in order to identify the link between aerosol hygroscopic properties, aerosol emission sources and particle formation mechanisms at the suburban area of Athens (fig. 8910B). The mean GF-PDFs were calculated for each cluster and for the different dry particle sizes (fig. 89A). Differences in mean GF between clusters were small, but trends in hygroscopicity across clusters were constituent for all particle sizes. Particle number size distributions vary across different regions and environments (Rose et al., 2021), and the structure of their patterns can be used as an indicator of the possible aerosol particle emission sources and formation processes. In DEM station,

secondary aerosol formation, mostly related to sulphate and organics, and traffic-related emissions are the main sources of ambient aerosol, while biomass burning also consists a major source in winter (Vratolis et al., 2019; Bousiotis et al., 2021; Tsiflikiotou et al., 2019; Kostenidou et al., 2015). In the present study, five clusters were identified which represent a combination of the major particle emission sources and formation/transformation processes. The modal characteristics of the clustered average number size distribution were summarized in Table S3. ~~In addition, for each cluster and dry particle size, (30, 50, 80 and 250nm), the hourly mean GF PDFs were calculated and presented in figure 10A.~~

~~Cluster analysis was performed on the hourly average size distributions to identify the link between ultrafine particle's hygroscopicity and dynamics.~~

~~The results are presented in Figure 11A. In addition, the temporal variation of occurrence of each cluster (fig. 11B) was put in context of wind direction data (fig. 11C5), to better interpret the possible sources of aerosol particles . Generally, the number size distributions vary significantly across different regions and environments (Rose et al., 2021). In Athens, secondary aerosol formation, mostly related to sulfate and organics, and traffic related emissions are the main sources affecting number concentration levels, while biomass burning also consists a major source of aerosol particles in winter. Specifically, in this study, five clusters were identified which represent the different particle emission sources and formation processes, (Vratolis et al., 2019; Bousiotis et al., 2021; Tsiflikiotou et al., 2019; Kostenidou et al., 2015). The modal characteristics of the clustered average number size distribution are summarized in Table S2.~~

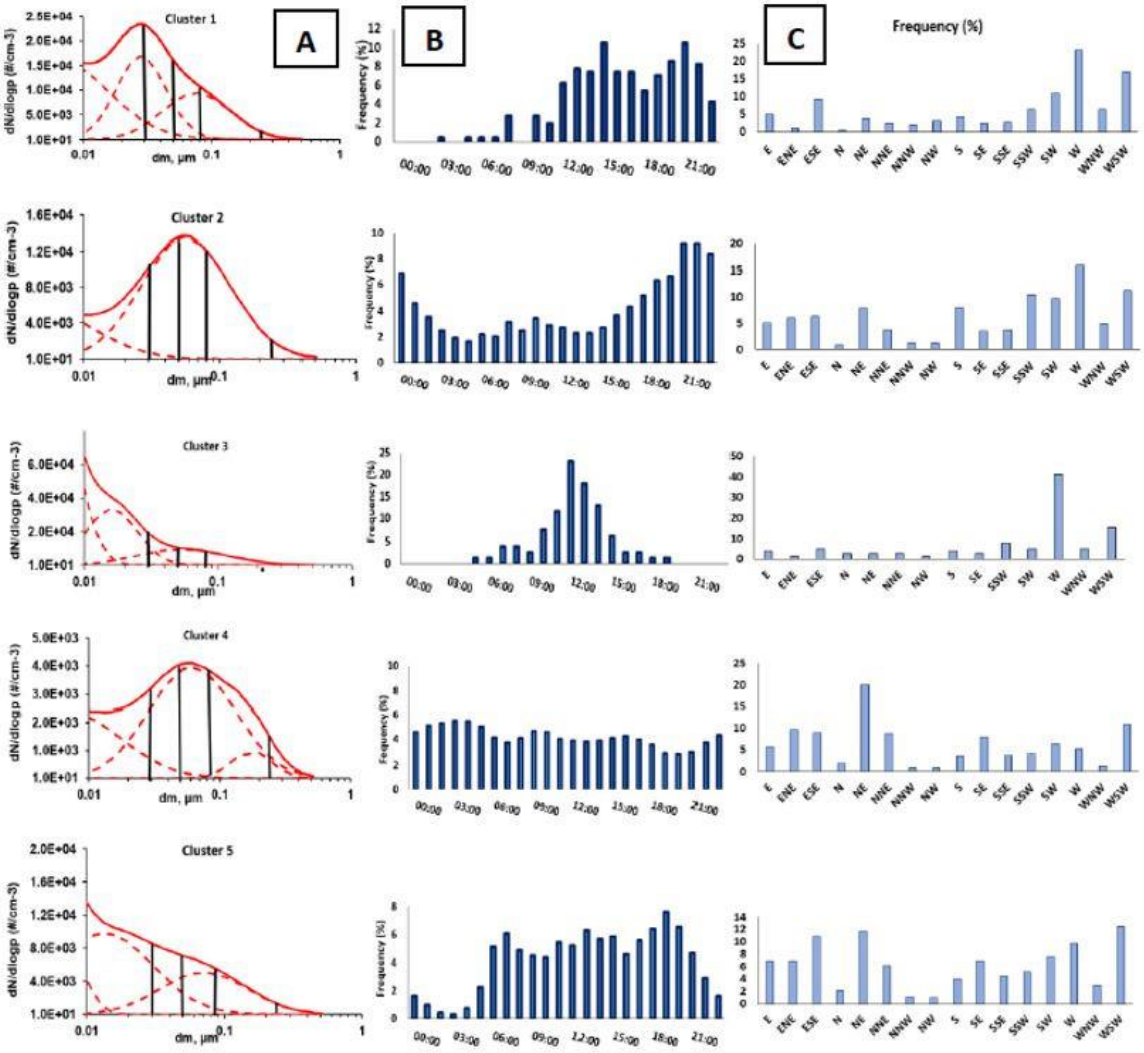
A
B
C
Cluster 1
Cluster 2
Cluster 3
Cluster 4
Cluster 5
dN/dlogp (#/cm-3)
dm, µm
Frequency (%)
00:00 03:00 06:00 09:00 12:00 15:00 18:00 21:00
E ENE ESE N NE NNE NNW NW S SE SSE SSW SW W WNW WSW

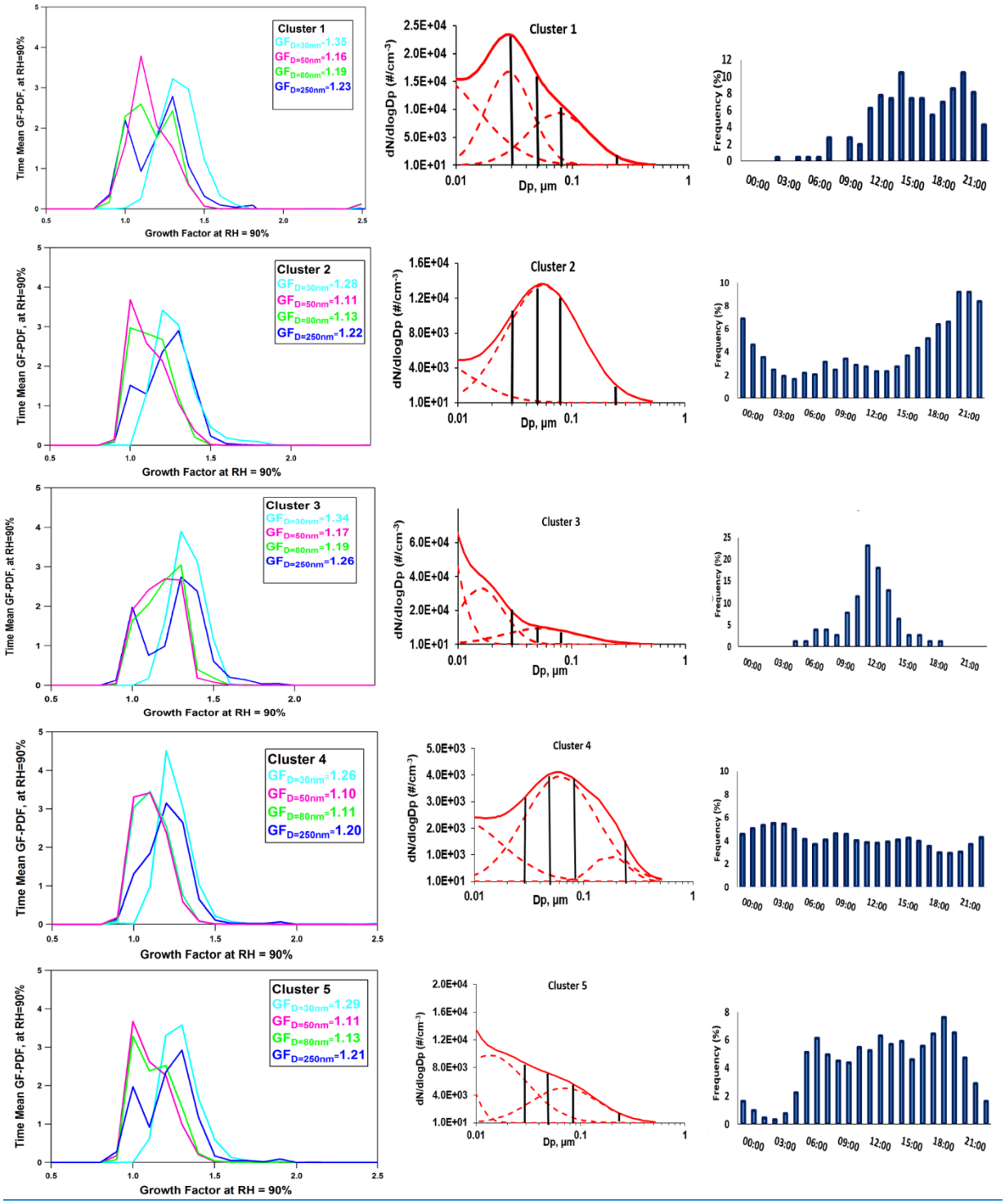

Figure ~~89~~101 A) Mean GF-PDF,B~~A~~) Average number size distribution and, C~~B~~) Hourly frequency of occurrence ~~and C) Frequency of wind direction~~ for each cluster.

Cluster 1 (Aged traffic mixed with background aerosol) accounts for 4.2 % of the hourly particle number size distributions. The fact that the frequency of the cluster occurrence peaks at noon and afternoon, while the morning traffic-related peak is missing, together with the prevailing westerly winds (fig. S5), hints to traffic-related pollution transported from the urban area. ~~This was also confirmed from the average number size distribution pattern. The average number size distribution has 3 modes (Table S3); one but less pronounced nuclei mode (d_p < 10 nm), a pronounced nuclei mode at 28 nm and a larger Aitken mode at 76 nm. The nuclei mode at 28 nm is probably related to freshly emitted soot particles, internally mixed with other aerosol species such as organics and sulfates, from the urban sector of Athens. These particles are hygroscopic with mean GF equal to 1.37 (Table S2). The larger Aitken particles represents an externally-mixed aerosol, also composed of a mixture of fresh (non-hygroscopic) and aged (slightly hygroscopic) particles from different combustion sources (e.g. traffic, biomass burning), the latter of which have undergone aerosol dynamic processing after emission (Brines et al., 2014; Hussein et al., 2014). Generally, the low growth factors are characteristic of polluted air masses (fresh soot from different combustion sources), while the "aging" of the particles makes them more hygroscopic (Vakeva et al., 2002).~~

Cluster 2 (urban, nocturnal) represents 12.1% of the hourly averaged number size distributions. The diurnal frequency of occurrence profile of this cluster is characterized by an evening peak. ~~(21:00 - 00:00 UTC).~~ The average particle number size ~~distribution has 2 modes; the~~ distribution has a major mode ~~appears~~ in the Aitken size range, ~~at 57 nm,~~ which is probably a synergetic effect ~~while a secondary and less pronounced mode appears in the nuclei size range (< 10 nm). During the evening hours, there is probably a synergetic effect~~ between particle emissions from different combustion sources and the development of the local inversion-nocturnal boundary layer. ~~The 30 nm particles were mostly internally mixed but less hygroscopic than the 30 nm particles of cluster 1, 3 and 5; The average GF was found equal to1.28. Only, 8% of these particles were externally mixed with average $GF_{\sim 1.12}$=1.07 and $GF_{\sim 1.12}$=1.23 (wintertime). The 50 nm Aitken particles were externally mixed with average growth factors 1.03, (non or slightly hygroscopic), and 1.21 (moderately hygroscopic).~~

Cluster 3 (Nucleation and growth) accounts for 1.3% of the hourly averaged number size distributions. The diurnal frequency of occurrence profile is characterized by a peak at noon and the nuclei mode at particle sizes < 10 nm seemed to contribute for more than 60% to the total number concentration. This cluster was characterized by the least frequency of occurrence but the highest total number concentration, and occurs almost exclusively under westerly wind directions (fig. S5), of low to moderately wind speeds; conditions that favour new particle nucleation. ~~The average particle number size distribution appeared to have 3 modes; one nuclei mode at size < 10 nm which contributed more than 60 % to the total number concentration, a second nuclei mode at 16 nm and an Aitken mode at 54 nm. The Aitken mode represents an external mixture of fresh and aged particles from incomplete combustion sources. Whereas, the 30 nm particles belong to larger nuclei mode (centered at16 nm), representing an internally mixed aerosol with mean GF equal to 1.35.~~

Cluster 4 (Urban and regional background) is the most frequent cluster (67%) and represents mainly the contribution of the ~~"~~regional/urban background aged aerosol~~"~~, mostly accounting for aged and long-range transported aerosols. The diurnal profile is characterized by an almost stable frequency of occurrence within the day, and minimum total number concentrations (Brines

et al., 2014). The major mode of the size distribution appeared in the Aitken size range (61 nm), while an additional mode also exists in the accumulation region.~~This cluster is characteristic of the atmospheric processes such as coagulation of ultrafine particles, condensation of gaseous precursors onto pre-existing particles and secondary aerosol formation. The average number size distribution is composed with 3 modes. The major mode appeared in the Aitken size range (61 nm), a secondary mode appeared in the nuclei size range (< 10 nm) while an additional mode also exists in the accumulation region (175 nm). The 30 nm particles belong to the Aitken mode and appeared to be internally mixed but less hygroscopic than the particles in the cluster 1, 3, and 5; The mean GF was equal to 1.26. Whereas, the 50 and 85 nm particles have similar GFs in all clusters.~~

Cluster 5 (Traffic fresh and further growth) has a frequency of occurrence of 15.3% and ~~. This specific cluster~~ is characterized by a peak in the frequency of occurrence during morning and late afternoon traffic rush hours, while an additional peak appeared at noon. It is not restricted to a specific wind direction, while the size distribution is similar to cluster 1 but with higher contribution of nuclei particles to the total particle number concentration.

~~Clusters 2, 4, and 5 are characterized by less hygroscopic particles compared to clusters 1 and 3. The mean GF-PDFs of the clusters 2 and 5 have similar patterns for the respective dry particle sizes.~~ Specifically~~Overall~~, clusters 2 and 5, which represent 12.1 % and 15.3% of the hourly averaged number size distributions, respectively have similar GF-PDFs patterns and average GFs values for all dry particle sizes. Clusters 1 and 3, which account only for 4.2 % and 1.3 % of the hourly particle number size distributions~~,~~ and are related with atmospheric conditions favoring new particle formation or transport of nuclei particles from the city center to the sampling site, ~~-~~were characterized by more hygroscopic particles (higher mean GFs) compared to the other clusters.~~,~~ The ~~while the~~ particles of cluster 4, which represent 67% of the averaged number size distributions, had the lowest mean~~average~~ GF values. The GF-PDF of the 30 nm appeared to have one moderately hygroscopic mode whose structure does not significantly between the clusters. For the larger particles, the distributions of the GFs appeared to have two modes with more of less distinct modes. In the case of cluster 4, which is mostly accounted for aged and long-range transported particles, the GF-PDFs of the Aitken particles appeared to have a broad mode with no distinct modes, whereas the particles in the accumulation mode appeared to have two modes but less distinct than in the other clusters.

~~The average number size distribution has 3 modes; one nuclei mode at sizes < 10 nm (major mode), probably formed from hot exhaust gases while the cool down and condense (Morawska et al., 2008; Baltensperger 2002), a larger nuclei mode at 14 nm (internally mixed) and one Aitken mode at 71 nm (externally mixed) having similar hygroscopic properties with the particles in clusters 1 and 3, even though being less hygroscopic especially in the case of the 30 nm particles. This seems reasonable since more oxidized organics and possible slightly more inorganics may contribute to the nuclei particles formed through photochemical driven nucleation compared to those formed through hot engine exhaust gas cooling. The average growth factor of the internally mixed 30 nm nucleation particles (upper tail of nuclei mode) was equal to 1.29, while the average growth factors of the externally mixed 30 nm (4 %) were $GF_{<1.12}$ = 1.07 and $GF_{>1.12}$ =1.20.~~

Conclusions

The h~~H~~ygroscopic properties of ambient aerosol were investigated ~~measured~~ at a suburban environment in Athens, over a period of 12 months, using an HTDMA system for dry particles sizes of 30 nm, 50 nm, 80 nm and 250 nm at relative humidity, (RH), of 90%. The standard deviation σ of the inverted GF-PDF was used as a measure of the mixing state of aerosol. The aerosol was characterized as internally, externally, (with two well-defined modes), or continuum of mixing states, (with two overlapping~~ed~~ modes). In the case of an externally mixed aerosol, the growth factor spectrum was characterized by a non and/or slightly hygroscopic mode, (e.g. black carbon, fresh carbonaceous aerosol), and a moderately hygroscopic mode, (e.g. aged traffic, ~~regional or~~ background aerosol).

The data were analyzed in term of their ~~with respect to~~ temporal seasonal and diurnal variability.~~; Although the modal GF was rather stable, the contribution of each mode of the GF spectrum to the total hygroscopicity showed a distinct variation.~~ The 30 nm particles were mostly internally mixed and moderately~~highly~~ hygroscopic in all seasons, ~~except from wintertime, when a significant fraction of non and/or slightly hygroscopic mode became distinct. This was attributed to the dominance of primary emissions from different combustion sources generally used for residential heating (e.g. wood burning) and the decline of the aging processes during this period.~~ The 50 nm and 80 nm Aitken particles were mostly externally mixed except from August when an internally mixed and non and/or slightly hygroscopic aerosol type dominated this size fraction~~all Aitken and larger fractions~~. The 250 nm particles were externally mixed, with the moderately hygroscopic mode being the major contributor to particle GFs, in all seasons. A higher degree of external mixing state in winter (February) was observed in all cases. This was generally expected due to the dominance of primary emissions from different combustion sources (i.e. biomass burning, traffic) and the less effective aging process under cold and dark conditions. Exact magnitude and timing at this seasonal effect remains elusive based on a single year of observations.

The number size distributions were also~~further~~ analyzed by means of cluster analysis to identify the link between aerosol hygroscopicity and state of mixing and ~~dynamics and~~ origin. The data were categorized into five clusters ~~5 groups~~ representative of ~~two~~ traffic-related emission sources, (fresh and aged traffic), the ~~regional/~~urban background~~,~~ and~~the~~ urban-nocturnal aerosol and the photochemically induced new particle formation (nucleation)~~. and growth.~~ The clusters related with atmospheric conditions favouring new particle formation or transport of nuclei particles from the city centre, after undergoing further mixing with the background aerosol, are characterized by more hygroscopic nuclei particles compared to the other clusters. The mean GF-PDFs of the Aitken particles and the particles in the accumulation size range revealed that their patterns are significantly associated with particle origin, being characterized by either a broad mode (urban and regional background aerosol), or two more or less distinct modes. ~~The mean GF was higher in the case of 30 nm particles, when a nuclei mode between 13 nm and 28 nm appeared in the number size distributions, implying that these particles might have originated from newly formed particles after aging and growth. The hygroscopic properties of the larger Aitken particles and the particles in accumulation mode do not significantly vary between the different clusters, apart from a slightly higher contribution of the hygroscopic mode in the case of the "mixed background aerosol" cluster which accounted for the 67 % of the size distributions.~~

The HTDMA data obtained in this study can be further parameterized and used as a proxy for CCN prediction.

Data Availability

Data are available upon request to the author (spitieri@ipta.demokritos.gr).

Competing Interest

The authors declare that they have no conflict of interest.

Author contributions

CS performed the formal analysis and wrote the original draft. CS and MG performed the investigation and data curation. CS, MG and MGB provided the methodology and conceptualization. KE, MGB and MG provided supervision and validation. MG, KE, and MGB contributed to reviewing and editing the manuscript.

Acknowledgement

This research is co-financed by Greece and the European Union (European Social Fund- ESF) through the Operational Programme «Human Resources Development, Education and Lifelong Learning» in the context of the project "Strengthening Human Resources Research Potential via Doctorate Research" (MIS-5000432), implemented by the State Scholarships Foundation (IKY).

We also acknowledge partial support by the project "PANhellenic infrastructure for Atmospheric Composition and climate change" (MIS 5021516), which is implemented under the Action "Reinforcement of the Research and Innovation Infrastructure", funded by the Operational Program "Competitiveness, Entrepreneurship and Innovation" (NSRF 2014-2020) and co-financed by Greece and the European Union (European Regional Development Fund).

We also acknowledge partial support by the Action titled "National Network on Climate Change and its Impacts - CLIMPACT", funded by the Public Investment Program of Greece, General Secretariat of Research and Technology/Ministry of Development and Investments".

References

Achtert, P., Birmili, W., Nowak, A., Wehner, B., Wiedensohler, A., Takegawa, N., Kondo, Y., Miyazaki, Y., Hu, M., and Zhu, T.: Hygroscopic growth of tropospheric particle number size distributions over the North China Plain, J. Geophys. Res., 114, D00G07, doi:10.1029/2008JD010921, 2009.

Baltensperger, Urs & Streit, N. & Weingartner, Ernest & Nyeki, S. & Prevot, Andre & Van Dingenen, Rita & Virkkula, Aki & Putaud, Jean Philippe & Even, A. & ten Brink, Harry & Blatter, A. & Neftel, Albrecht & Gaeggeler, Heinz.: Urban and

rural aerosol characterization of summer smog events during the PIPAPO field campaign in Milan, Italy. Journal of Geophysical Research. 107. 10.1029/2001JD001292, 2002.

Bernardoni, V., Elser, M., Valli, G., Valentini, S., Bigi, A., Fermo, P., Piazzalunga, A., Vecchi, R., Size-segregated aerosol in a hot-spot pollution urban area: Chemical composition and three-way source apportionment, (2017) Environmental Pollution, 231, pp. 601-61, 2017.

Bezantakos, S., Barmpounis, K., Giamarelou, M., Bossioli, E., Tombrou, M., Mihalopoulos, N., Eleftheriadis, K., Kalogiros, J., D. Allan, J., Bacak, A., Percival, C. J., Coe, H., and Biskos, G.: Chemical composition and hygroscopic properties of aerosol particles over the Aegean Sea, Atmos. Chem. Phys., 13, 11595–11608, https://doi.org/10.5194/acp-13-11595-2013, 2013.

Bourcier, L., Sellegri, K., Chausse, P. et al. Seasonal variation of water-soluble inorganic components in aerosol size-segregated at the puy de Dôme station (1,465 m a.s.l.), France. J AtmosChem69, 47–66,https://doi.org/10.1007/s10874-012-9229-2, 2012.

Bougiatioti, A., Bezantakos, S., Stavroulas, I., Kalivitis, N., Kokkalis, P., Biskos, G., Mihalopoulos, N., Papayannis, A., and Nenes, A.: Biomass-burning impact on CCN number, hygroscopicity and cloud formation during summertime in the eastern Mediterranean, Atmos. Chem. Phys., 16, 7389–7409, https://doi.org/10.5194/acp-16-7389-2016, 2016.

Bousiotis, D., Pope D., F., Beddows, C. S. D., Dall'Osto. M., Massling, A., Nøjgaard, K. J., Nordstrøm, C., Niemi, V. J., Portin, H., Petäjä, T., Perez, N., Alastuey, A., Querol, X., Kouvarakis, G., Mihalopoulos, N., Vratolis, S., Eleftheriadis, K., Wiedensohler,A., Weinhold, K., Merkel, M., Tuch, T., and Harrison M. R., Atmos. Chem. Phys., 21, 11905–11925, https://doi.org/10.5194/acp-21-11905-2021, 2021

Brines, M. Dall'Osto, M., Beddows, D.C.S., Harrison, R. M., and Querol, X., Simplifying aerosol size distributions modes simultaneously detected at four monitoring sites during SAPUSS. Atmos. Chem. Phys., 14, 2973–2986, 2014.

Carrico, C. M.; Kreidenweis, S. M.; Malm, W. C.; Day, D. E.; Lee, T.; Carrillo, J.; McMeeking, G. R.; Collett, J. L. Hygroscopic growth behavior of a carbon-dominated aerosol in Yosemite National Park Atmos. Environ., 39 1393 1404, 2005.

Cubison, M. J., Alfarra, M. R., Allan, J., Bower, K. N., Coe, H., McFiggans, G. B., Whitehead, J. D., Williams, P. I., Zhang, Q., Jimenez, J. L., Hopkins, J., and Lee, J.: The characterization of pollution aerosol in a changing photochemical environment, Atmos. Chem. Phys., 6, 5573–5588, https://doi.org/10.5194/acp-6-5573-2006, 2006.

Carslaw, D. C. and Ropkins, K.: openair –An R package for air quality data analysis, Environ. Model. Softw., 27–28, 52–61, https://doi.org/10.1016/j.envsoft.2011.09.008, 2012

Dean A. Hegg, David S. Covert, Haflidi Jonsson, Paul A. Covert.: An Instrument for Measuring Size-Resolved Aerosol Hygroscopicity at both Sub- and Super-MicronSizes, Aerosol Science and Technology, 41:9, 873-883, DOI: 10.1080/02786820701506955, 2007.

David R. Cocker III, Nathan E. Whitlock, Richard C. Flagan& John H. Seinfeld.: Hygroscopic Properties of Pasadena, California Aerosol,Aerosol Science and Technology,35:2,637-647,DOI: 10.1080/02786820120653, 2001.

Diapouli, E.; Kalogridis, A.-C.; Markantonaki, C.; Vratolis, S.; Fetfatzis, P.; Colombi, C.; Eleftheriadis, K. Annual Variability of Black Carbon Concentrations Originating from Biomass and Fossil Fuel Combustion for the Suburban Aerosol in Athens, Greece. Atmosphere 2017, 8, 234. https://doi.org/10.3390/atmos8120234, 2017.

Eleftheriadis, K., Gini, M.I., Diapouli, Vratolis S., Vasilatou V., Fetfatzis P., Manousakkas I. M.:. Aerosol microphysics and chemistry reveal the COVID19 lockdown impact on urban air quality. Scientific Reports 11, 14477, https://doi.org/10.1038/s41598-021-93650-6, 2021.

Enroth, J., Mikkilä, J., Németh, Z., Kulmala, M., and Salma, I.: Wintertime hygroscopicity and volatility of ambient urban aerosol particles, Atmos. Chem. Phys., 18, 4533–4548, https://doi.org/10.5194/acp-18-4533-2018, 2018.

Fors, E. O., Swietlicki, E., Svenningsson, B., Kristensson, A., Frank, G. P., and Sporre, M.: Hygroscopic properties of the ambient aerosol in southern Sweden – a two year study, Atmos. Chem. Phys., 11, 8343–8361, https://doi.org/10.5194/acp-11-8343-2011, 2011.

Gunthe, S. S., King, S. M., Rose, D., Chen, Q., Roldin, P., Farmer, D. K., Jimenez, J. L., Artaxo, P., Andreae, M. O., Martin, S. T., and Pöschl, U.: Cloud condensation nuclei in pristine tropical rainforest air of Amazonia: size-resolved measurements and modeling of atmospheric aerosol composition and CCN activity, Atmos. Chem. Phys., 9, 7551–7575, https://doi.org/10.5194/acp-9-7551-2009, 2009.

Gysel, M., Crosier, J., Topping, D. O., Whitehead, J. D., Bower, K. N., Cubison, M. J., Williams, P. I., Flynn, M. J., McFiggans, G. B., and Coe, H.: Closure study between chemical composition and hygroscopic growth of aerosol particles during TORCH2, Atmos. Chem. Phys., 7, 6131–6144, https://doi.org/10.5194/acp-7-6131-2007, 2007.

Gysel, M., McFiggans, G.B., Coe, H., Inversion of tandem differential mobility analyser (TDMA) measurements, Journal of Aerosol Science, Volume 40, Issue 2, 134-151, ISSN 0021-8502, https://doi.org/10.1016/j.jaerosci.2008.07.013, 2009.

Gysel M, Weingartner E, Baltensperger U. Hygroscopicity of aerosol particles at low temperatures. 2. Theoretical and experimental hygroscopic properties of laboratory generated aerosols. Environ Sci Technol. 2002 Jan 1;36(1):63-8. doi: 10.1021/es010055g. PMID: 11811491, 2002.

Haywood, J., and Boucher, O.: Estimates of the direct and indirect radiative forcing due to tropospheric aerosols: A review, Rev. Geophys., 38(4), 513– 543, doi:10.1029/1999RG000078, 2000.

Hussein T., Mølgaard, B., Hannuniemi, H., Martikainen, J., Järvi, L., Wegner, T., Ripamonti, G., Weber, S., Vesala, T. & Hämeri, K.: Fingerprints of the urban particle number size distribution in helsinki, Finland: local versus regional characteristics. Boreal Env. Res. 19: 1–20, 2014.

Hussein T., Hämeri K., Aalto P., Paatero P., Kulmala M., Modal structure and spatial–temporal variations of urban and suburban aerosols in Helsinki—Finland, Atmospheric Environment, Volume 39, Issue 9, Pages 1655-1668, ISSN 1352-2310, https://doi.org/10.1016/j.atmosenv.2004.11.031, 2005.

Holmgren, H., Sellegri, K., Hervo, M., Rose, C., Freney, E., Villani, P., and Laj, P.: Hygroscopic properties and mixing state of aerosol measured at the high-altitude site Puy de Dôme (1465 m a.s.l.), France, Atmos. Chem. Phys., 14, 9537–9554, https://doi.org/10.5194/acp-14-9537-2014, 2014.

IPCC: Climate Change 2013: The Physical Science Basis. Contribution of Working Group I to the Fifth Assessment Report of the Intergovernmental Panel on Climate Change, Cambridge University Press, Cambridge, UK and Neew York, NY, USA, 2013.

Jurányi, Z., Tritscher, T., Gysel, M., Laborde, M., Gomes, L., Roberts, G., Baltensperger, U., and Weingartner, E.: Hygroscopic mixing state of urban aerosol derived from size-resolved cloud condensation nuclei measurements during the MEGAPOLI campaign in Paris, Atmos. Chem. Phys., 13, 6431–6446, https://doi.org/10.5194/acp-13-6431-2013, 2013.

Kammermann, L., Gysel, M., Weingartner, E., and Baltensperger, U.: 13-month climatology of the aerosol hygroscopicity at the free tropospheric site Jungfraujoch (3580 m a.s.l.), Atmos. Chem. Phys., 10, 10717–10732, https://doi.org/10.5194/acp-10-10717-2010, 2010.

Kanakidou, M., Seinfeld, J. H., Pandis, S. N., Barnes, I., Dentener, F. J., Facchini, M. C., Van Dingenen, R., Ervens, B., Nenes, A., Nielsen, C. J., Swietlicki, E., Putaud, J. P., Balkanski, Y., Fuzzi, S., Horth, J., Moortgat, G. K., Winterhalter, R., Myhre, C. E. L., Tsigaridis, K., Vignati, E., Stephanou, E. G., and Wilson, J.: Organic aerosol and global climate modelling: a review, Atmos. Chem. Phys., 5, 1053–1123, https://doi.org/10.5194/acp-5-1053-2005, 2005.

Kalivitis, N., Kerminen, V.-M., Kouvarakis, G., Stavroulas, I., Bougiatioti, A., Nenes, A., Manninen, H. E., Petäjä, T., Kulmala, M., and Mihalopoulos, N.: Atmospheric new particle formation as a source of CCN in the eastern Mediterranean marine boundary layer, Atmos. Chem. Phys., 15, 9203–9215, https://doi.org/10.5194/acp-15-9203-2015, 2015.

Kaufman, Y., Tanré, D. & Boucher, O. A satellite view of aerosols in the climate system. Nature 419, 215–223, https://doi.org/10.1038/nature01091, 2002.

Kalogridis, A. C., Vratolis, S., Liakakou, E., Gerasopoulos, E., Mihalopoulos, N., and Eleftheriadis, K., Assessment of wood burning versus fossil fuel contribution to wintertime black carbon and carbon monoxide concentrations in Athens, Greece, Atmos. Chem. Phys., 18, 10219–10236, 2018, https://doi.org/10.5194/acp-18-10219-2018.

Kim, N., Yum, S. S., Park, M., Park, J. S., Shin, H. J., and Ahn, J. Y.: Hygroscopicity of urban aerosols and its link to size-resolved chemical composition during spring and summer in Seoul, Korea, Atmos. Chem. Phys., 20, 11245–11262, https://doi.org/10.5194/acp-20-11245-2020, 2020.

~~Kim N., Seong Soo Yum, Minsu Park, Jong Sung Park, Hye Jung Shin, and Joon Young Ahn, Atmos. Chem. Phys., 20, 11245-11262, 2020https://doi.org/10.5194/acp-20-11245-2020, 2020.~~

Koehler, K. A., Kreidenweis, S. M., DeMott, P. J., Prenni, A. J., Carrico, C. M., Ervens, B., and Feingold, G.: Water activity and activation diameters from hygroscopicity data - Part II: Application to organic species, Atmos. Chem. Phys., 6, 795–809, https://doi.org/10.5194/acp-6-795-2006, 2006.

Köhler, H.: The nucleous in the growth of hygroscopic droplets, Trans. Faraday Soc., 32, 1152-1161, 1936.

Kostenidou, E., Florou, K., Kaltsonoudis, C., Tsiflikiotou, M., Vratolis, S., Eleftheriadis, K., and Pandis, S. N.: Sources and chemical characterization of organic aerosol during the summer in the eastern Mediterranean, Atmos. Chem. Phys., 15, 11355–11371, https://doi.org/10.5194/acp-15-11355-2015, 2015.

Kotchenruther, R. A. & Hobbs, P. V. Humidification factors of aerosols from biomass burning in Brazil. J. Geophys. Res. Atmospheres 103, 32081–32089, 1998.

Petters, M. D., and S. M. Kreidenweis (2007), A single parameter representation of hygroscopic growth and cloud condensation nucleus activity, Atmos. Chem. Phys., 7(8), 1961–1971, 2007.

Z. L. Li, ~~Zhanqing Lau,~~ W. K.-M.Ramanathan, V.Wu, G.Ding, Y.Manoj, M. G.Liu, J.Qian, Y.Li, J.Zhou, T.Fan, J.Rosenfeld, D.Ming, Y.Wang, Y.Huang, J.Wang, B.Xu, X.Lee, S.-S.Cribb, M.Zhang, F.Yang, X.Zhao, C.Takemura, T.Wang, K.Xia, X.Yin, Y.Zhang, H.Guo, J.Zhai, P. M.Sugimoto, N.Babu, S. S.Brasseur, G. P.:Aerosol and monsoon climate interactions over Asia, Rev. Geophys., 54, 866– 929, doi:10.1002/2015RG000500, 2016.

~~Laborde, M., Crippa, M., Tritscher, T., Jurányi, Z., Decarlo, P. F., Temime-Roussel, B., Marchand, N., Eckhardt, S., Stohl, A., Baltensperger, U., Prévôt, A. S. H., Weingartner, E., and Gysel, M.: Black carbon physical properties and mixing state in the European megacity Paris, Atmos. Chem. Phys., 13, 5831–5856, https://doi.org/10.5194/acp-13-5831-2013, 2013.~~

McFiggans, G., Artaxo, P., Baltensperger, U., Coe, H., Facchini, M. C., Feingold, G., Fuzzi, S., Gysel, M., Laaksonen, A., Lohmann, U., Mentel, T. F., Murphy, D. M., O'Dowd, C. D., Snider, J. R., and Weingartner, E.: The effect of physical and chemical aerosol properties on warm cloud droplet activation, Atmos. Chem. Phys., 6, 2593–2649, https://doi.org/10.5194/acp-6-2593-2006, 2006.

Massling, A., Leinert, S., Wiedensohler, A., and Covert, D.: Hygroscopic growth of sub-micrometer and one-micrometer aerosol particles measured during ACE-Asia, Atmos. Chem. Phys., 7, 3249–3259, https://doi.org/10.5194/acp-7-3249-2007, 2007.

Mochida, Michihiro & Miyakawa, Takuma & Takegawa, Nobuyuki & Morino, Yu & Kawamura, Kimitaka & Kondo, Yutaka.: Significant alteration in the hygroscopic properties of urban aerosol particles by the secondary formation of organics. Geophys. Res. Lett. 35. 10.1029/2007GL031310, 2008.

~~Morawska, L., Ristovski, Z., Jayaratne, E.R., Keogh, D.U., Ling, X.: Ambient nano and ultrafine particles from motor vehicle emissions: Characteristics, ambient processing and implications on human exposure. Atmos. Environ. 42, 8113–8138. https://doi.org/10.1016/j.atmosenv.2008.07.050, 2008.~~

Motos, G., Schmale, J., Corbin, J. C., Zanatta, M., Baltensperger, U., and Gysel-Beer, M.: Droplet activation behaviour of atmospheric black carbon particles in fog as a function of their size and mixing state. Atmos. Chem. Phys., 19, 2183-2207, doi:10.5194/acp-19-2183-2019, 2019.

~~Kim, N., Yum, S. S., Park, M., Park, J. S., Shin, H. J., and Ahn, J. Y.: Hygroscopicity of urban aerosols and its link to size-resolved chemical composition during spring and summer in Seoul, Korea, Atmos. Chem. Phys., 20, 11245–11262, https://doi.org/10.5194/acp-20-11245-2020, 2020.~~

Paramonov, M., Kerminen, V.-M., Gysel, M., Aalto, P. P., Andreae, M. O., Asmi, E., Baltensperger, U., Bougiatioti, A., Brus, D., Frank, G. P., Good, N., Gunthe, S. S., Hao, L., Irwin, M., Jaatinen, A., Jurányi, Z., King, S. M., Kortelainen, A., Kristensson, A., Lihavainen, H., Kulmala, M., Lohmann, U., Martin, S. T., McFiggans, G., Mihalopoulos, N., Nenes, A., O'Dowd, C. D., Ovadnevaite, J., Petäjä, T., Pöschl, U., Roberts, G. C., Rose, D., Svenningsson, B., Swietlicki, E., Weingartner,

E., Whitehead, J., Wiedensohler, A., Wittbom, C., and Sierau, B.: A synthesis of cloud condensation nuclei counter (CCNC) measurements within the EUCAARI network, Atmos. Chem. Phys., 15, 12211–12229, https://doi.org/10.5194/acp-15-12211-2015, 2015.

Psichoudaki M., Nenes A., Florou K., Kaltsonoudis C., Pandis N.S.,: Hygroscopic properties of atmospheric particles emitted during wintertime biomass burning episodes in Athens, Atmospheric Environment, Volume 178, 2018, Pages 66-72, ISSN 1352-2310, https://doi.org/10.1016/j.atmosenv.2018.01.004, 2018.

Petters, M. D. AND Kreidenweis, S.M.: A single parameter representation of hygroscopic growth and cloud condensation nucleus activity, Atmos. Chem. Phys., 7, 1961-1971, doi:10.5194/acp-7-1961-2007, 2007.

Petäjä, T., Kerminen, V.-M., Dal Maso, M., Junninen, H., Koponen, I. K., Hussein, T., Aalto, P. P., Andronopoulos, S., Robin, D., Hämeri, K., Bartzis, J. G., and Kulmala, M.: Sub-micron atmospheric aerosols in the surroundings of Marseille and Athens: physical characterization and new particle formation, Atmos. Chem. Phys., 7, 2705–2720, https://doi.org/10.5194/acp-7-2705-2007, 2007.

~~Rose, D., Achtert, P., Nowak, A. Wiedensohler, A., Hu, M., Shao, M., Zhang, Y., Andreae, M. O., and Pöschl, U., Cloud condensation nuclei in polluted air and biomass burning smoke: Size-resolved measurements and implications for the modeling of aerosol particle hygroscopicity and CCN activity, Geophysical Research Abstracts, Vol. 11, EGU2009-10312, 2009 EGU General Assembly, 2009.~~

~~Rose, D., Nowak, A., Achtert, P., Wiedensohler, A., Hu, M., Shao, M., Zhang, Y., Andreae, M. O., and Pöschl, U.: Cloud condensation nuclei in polluted air and biomass burning smoke near the mega-city Guangzhou, China – Part 1: Size-resolved measurements and implications for the modeling of aerosol particle hygroscopicity and CCN activity, Atmos. Chem. Phys., 10, 3365–3383, https://doi.org/10.5194/acp-10-3365-2010, 2010.~~

Rose, C., Collaud Coen, M., Andrews, E., Lin, Y., Bossert, I., Lund Myhre, C., Tuch, T., Wiedensohler, A., Fiebig, M., Aalto, P., Alastuey, A., Alonso-Blanco, E., Andrade, M., Artíñano, B., Arsov, T., Baltensperger, U., Bastian, S., Bath, O., Beukes, J. P., Brem, B. T., Bukowiecki, N., Casquero-Vera, J. A., Conil, S., Eleftheriadis, K., Favez, O., Flentje, H., Gini, M. I., Gómez-Moreno, F. J., Gysel-Beer, M., Hallar, A. G., Kalapov, I., Kalivitis, N., Kasper-Giebl, A., Keywood, M., Kim, J. E., Kim, S.-W., Kristensson, A., Kulmala, M., Lihavainen, H., Lin, N.-H., Lyamani, H., Marinoni, A., Martins Dos Santos, S., Mayol-Bracero, O. L., Meinhardt, F., Merkel, M., Metzger, J.-M., Mihalopoulos, N., Ondracek, J., Pandolfi, M., Pérez, N., Petäjä, T., Petit, J.-E., Picard, D., Pichon, J.-M., Pont, V., Putaud, J.-P., Reisen, F., Sellegri, K., Sharma, S., Schauer, G., Sheridan, P., Sherman, J. P., Schwerin, A., Sohmer, R., Sorribas, M., Sun, J., Tulet, P., Vakkari, V., van Zyl, P. G., Velarde, F., Villani, P., Vratolis, S., Wagner, Z., Wang, S.-H., Weinhold, K., Weller, R., Yela, M., Zdimal, V., and Laj, P.: Seasonality of the particle number concentration and size distribution: a global analysis retrieved from the network of Global Atmosphere Watch (GAW) near-surface observatories, Atmos. Chem. Phys., 21, 17185–17223, https://doi.org/10.5194/acp-21-17185-2021, 2021.

Riemer, N., Ault, A. P., West, M., Craig, R. L., & Curtis, J. H.: Aerosol mixing state: Measurements, modeling, and impacts. Reviews of Geophysics, 57, 187–249. https://doi. org/10.1029/2018RG000615, 2019.

Rickards, Andrew M. J. Miles, Rachael E. H. Davies, James F. Marshall, Frances H. Reid, Jonathan P. :Measurements of the Sensitivity of Aerosol Hygroscopicity and the κ Parameter to the O/C Ratio, J. Phys. Chem. A 2013, 117, 51, 14120–14131, https://doi.org/10.1021/jp407991n, 2013.

Rosenfeld, D., Andreae, M. O., Asmi, A., Chin, M., Leeuw, G., Donovan, D. P., Kahn, R., Kinne, S., Kivekäs, N., Kulmala, M., Lau, W., Schmidt, K. S., Suni, T., Wagner, T., Wild, M., Quaas, J.: Global observations of aerosol-cloud-precipitation-climate interactions, Rev. Geophys., 52, 750– 808, doi:10.1002/2013RG000441, 2014.

Sjogren, S., Gysel, M., Weingartner, E., Alfarra, M. R., Duplissy, J., Cozic, J., Crosier, J., Coe, H., and Baltensperger, U.: Hygroscopicity of the submicrometer aerosol at the high-alpine site Jungfraujoch, 3580 m a.s.l., Switzerland, Atmos. Chem. Phys., 8, 5715–5729, https://doi.org/10.5194/acp-8-5715-2008, 2008.

Tsiflikiotou, M.A., Kostenidou, E., Papanastasiou, D.K., Patoulias, D., Zarmpas, P., Paraskevopoulou, D., Diapouli, E., Kaltsonoudis, C., Florou, K., Bougiatioti, A., Stavroulas, I., Theodosi, C., Kouvarakis, G., Vasilatou, V., Siakavaras, D., Biskos, G., Pilinis, C., Eleftheriadis, K., Gerasopoulos, E., Mihalopoulos, N., Pandis, S.N. (2019) Summertime particulate matter and its composition in Greece. *Atmospheric Environment*, 213. 597-607 doi:10.1016/j.atmosenv.2019.06.013.

Schmale, J., Henning, S., Henzing, B., Gysel, M.: Collocated observations of cloud condensation nuclei, particle size distributions, and chemical composition. *Sci. Data* 4,170003, doi: 10.1038/sdata.2017.3, 2017.

Schmale, J., Henning, S., Decesari, S., Henzing, B., Keskinen, H., Sellegri, K., Ovadnevaite, J., Pöhlker, M. L., Brito, J., Bougiatioti, A., Kristensson, A., Kalivitis, N., Stavroulas, I., Carbone, S., Jefferson, A., Park, M., Schlag, P., Iwamoto, Y., Aalto, P., Äijälä, M., Bukowiecki, N., Ehn, M., Frank, G., Fröhlich, R., Frumau, A., Herrmann, E., Herrmann, H., Holzinger, R., Kos, G., Kulmala, M., Mihalopoulos, N., Nenes, A., O'Dowd, C., Petäjä, T., Picard, D., Pöhlker, C., Pöschl, U., Poulain, L., Prévôt, A. S. H., Swietlicki, E., Andreae, M. O., Artaxo, P., Wiedensohler, A., Ogren, J., Matsuki, A., Yum, S. S., Stratmann, F., Baltensperger, U., and Gysel, M.: Long-term cloud condensation nuclei number concentration, particle number size distribution and chemical composition measurements at regionally representative observatories, Atmos. Chem. Phys., 18, 2853–2881, https://doi.org/10.5194/acp-18-2853-2018, 2018.

Swietlicki, E., Hansson, H-C., Hameri, K., Svenningsson, B., Massling, A., McFiggans, G., McMurry, P. H., Petäjä, T., Tunved, P., Gysel, M., Topping, D., Weingartner, E., Baltensperger, U., Rissler, J., Wiedensohler, A., & Kulmala, M.:Hygroscopic properties of submicrometer atmospheric aerosol particles measured with H-TDMA instruments in various environments - a review. Tellus. Series B: Chemical and Physical Meteorology, 60(3), 432-469. https://doi.org/10.1111/j.1600-0889.2008.00350.x, 2008

Tritscher, T., Dommen, J., DeCarlo, P. F., Gysel, M., Barmet, P. B., Praplan, A. P., Weingartner, E., Prévôt, A. S. H., Riipinen, I., Donahue, N. M., and Baltensperger, U.: Volatility and hygroscopicity of aging secondary organic aerosol in a smog chamber, Atmos. Chem. Phys., 11, 11477–11496, https://doi.org/10.5194/acp-11-11477-2011, 2011.

Vratolis S., Gini M. I., Bezentakos S., Stavroulas I., Kalivitis N., Kostenidou E., Louvaris E., Siakavaras D. Biskos G., Mihalopoulos N., Pandis S. N., Pilinis C., Papayannis A., and Eleftheriadis K.: Particle number size distribution statistics at city-centre, urban background, and remote stations in Greece during summer, Atmos. Environ., 213, 711-726, 2019.

Vu, T.V., Shi, Z. & Harrison, R.M. Estimation of hygroscopic growth properties of source-related sub-micrometre particle types in a mixed urban aerosol, Clim. Atmos. Sci. 4, 21, https://doi.org/10.1038/s41612-021-00175-w, 2021.

Vlasenko, S. Sjögren, E. Weingartner, H. W. Gäggeler & M. Ammann.: Generation of Submicron Arizona Test Dust Aerosol: Chemical and Hygroscopic Properties, Aerosol Science and Technology,39:5,452-460,DOI: 10.1080/027868290959870, 2005.

~~Vakeva, M., K. Hameri, and P. P. Aalto: Hygroscopic properties of nucleation mode and Aitken mode particles during nucleation bursts and in background air on the west coast of Ireland, J. Geophys. Res., 107(D19), 8104, doi:10.1029/2000JD000176, 2002.~~

-Wang, X., Shen, X. J., Sun, J.Y., Zhang, X.Y., Wang, Y.Q., Zhang, Y. M., Wang, P., Xia, C., Qi, X. F., Zhong, J. T.: Size-resolved hygroscopic behavior of atmospheric aerosols during heavy aerosol pollution episodes in Beijing in December 2016, Atmospheric Environment, Volume 194, 2018, Pages 188-197, ISSN 1352-2310, https://doi.org/10.1016/j.atmosenv.2018.09.041, 2018.

Wiedensohler, A., Birmili, W., Nowak, A., Sonntag, A., Weinhold, K., Merkel, M., Wehner, B., Tuch, T., Pfeifer, S., Fiebig, M., Fjäraa, A. M., Asmi, E., Sellegri, K., Depuy, R., Venzac, H., Villani, P., Laj, P., Aalto, P., Ogren, J. A., Swietlicki, E., Williams, P., Roldin, P., Quincey, P., Hüglin, C., Fierz-Schmidhauser, R., Gysel, M., Weingartner, E., Riccobono, F., Santos, S., Grüning, C., Faloon, K., Beddows, D., Harrison, R., Monahan, C., Jennings, S. G., O'Dowd, C. D., Marinoni, A., Horn, H.-G., Keck, L., Jiang, J., Scheckman, J., McMurry, P. H., Deng, Z., Zhao, C. S., Moerman, M., Henzing, B., de Leeuw, G., Löschau, G., and Bastian, S.: Mobility particle size spectrometers: harmonization of technical standards and data structure to facilitate high quality long-term observations of atmospheric particle number size distributions, Atmos. Meas. Tech., 5, 657–685, https://doi.org/10.5194/amt-5-657-2012, 2012.

Xu, W., Sun, Y., Wang, Q., Zhao, J., Wang, J., Ge, X., Xie, C., Zhou, W., Du, W., Li, J., Fu, P., Wang, Z., Worsnop, R. D., Coe, H.: Changes in aerosol chemistry from 2014 to 2016 in winter in Beijing: Insights from high-resolution aerosol mass spectrometry. Journal of Geophysical Research: Atmospheres, 124, 1132– 1147. https://doi.org/10.1029/2018JD029245, 2019.

Zhang, Q., Jimenez, J. L., Canagaratna, M. R., Ulbrich, I. M., Ng, N. L., Worsnop, D. R., Sun, Y.,: Understanding atmospheric organic aerosols via factor analysis of aerosol mass spectrometry: a review. Anal BioanalChem401, 3045–3067,https://doi.org/10.1007/s00216-011-5355-y, 2011.